Technical Memo

ECMWF
European Centre for Medium-Range Weather Forecasts

886

Investigating the use of Lambertian reflection in the assimilation of surface-sensitive microwave sounding radiances over snow and sea-ice

Niels Bormann

September 2021

Series: ECMWF Technical Memoranda

A full list of ECMWF Publications can be found on our web site under:
http://www.ecmwf.int/en/publications/

Contact: library@ecmwf.int

Abstract

This paper investigates two aspects aimed at an increased use of surface-sensitive microwave sounding radiances for NWP, namely the assimilation of humidity-sounding radiances from ATMS over snow, as well as the use of Lambertian reflection in the radiative transfer modelling over snow and sea-ice surfaces. The Lambertian characteristics are modelled through a parameterisation of the effective zenith angle used to calculate the down-welling radiation in the radiative transfer model.

Using Lambertian rather than specular reflection significantly improves the forward modelling for 183 GHz humidity-sounding channels over snow and sea-ice in comparisons to observations, including a reduction of significant zenith-angle dependent biases. For temperature-sounding channels in the 50 GHz band, comparisons between observations and background equivalents also suggest improvements from treating snow and sea-ice surfaces as Lambertian or semi-Lambertian, but the characteristics appear more variable, and there are indications of other sources of error such as biases in the skin-temperature. For both spectral regions the improvement from using non-specular reflection is clearest for snow-covered land surfaces.

Assimilation experiments show that the addition of 183 GHz humidity-sounding channels from ATMS over snow-covered land lead to a slight positive impact over the higher latitudes in winter. On top of this, replacing the specular surface assumption over snow and sea-ice with a fully Lambertian for 183 GHz channels on ATMS and semi-Lambertian for 50 Ghz channels on ATMS and AMSU-A means that more observations pass quality control, giving a neutral to slightly positive impact at higher latitudes in winter. Combining the two changes leads to small forecast benefits that are statistically significant up to day 3 at higher latitudes.

1 Introduction

Sounding radiances from passive microwave (MW) instruments contribute strongly to today's skill of medium-range weather forecasts (Bormann et al. 2019). This is due to a number of factors, including the present availability of a comparatively large number of sensors with reliable quality (Duncan and Bormann 2020), our ability to use the observations in a wide range of atmospheric conditions (incl. cloudy and rainy scenes, Geer et al. 2017)), and an adequate forward modelling and uncertainty treatment for most situations. Observations over the free ocean contribute particularly strongly, enabled by relatively low uncertainties in the forward modelling of the surface-related aspects (e.g., Liu et al. 2011). MW sounding radiances are also assimilated over land and sea-ice regions, where they also provide clear forecast benefits, including from observations sensitive to the surface (Bormann et al. 2017), even though surface-related uncertainties are larger.

Recent studies, however, highlight that less impact is found from MW radiances in the Northern Hemisphere during winter (Lawrence et al. 2019, Bormann et al. 2019, Bormann et al. 2017), and this has been at least partly attributed to a poorer use of the observations over snow and sea-ice regions. In these regions, many surface-sensitive MW radiances are presently rejected, as the background estimates of the observations deviates too much from the observed values or uncertainty estimates are considered too large. Where observations are not rejected by quality control, there tend to be larger biases between the observations and the background (e.g., Lawrence et al. 2019). Both of these aspects highlight deficiencies in the modelling of the observations.

Several aspects contribute to a sub-optimal use and modelling of surface-sensitive MW sounding radiances over snow and sea-ice. The representation of the surface conditions in the radiative transfer is highly simplified, based on an effective skin temperature and an effective surface emissivity. For the

former, it is assumed that the model temperature of the top-level provides an adequate initial estimate, and this may not be the case for MW frequencies over snow and sea-ice, as it neglects penetration effects (e.g., Bormann et al. 2017, Harlow 2009). In addition, specular surface reflection is assumed, while this may be a poor assumption over snow and sea-ice surfaces (e.g., Guedj et al. 2010, Harlow 2009, Rosenkranz and Mätzler 2008, Mätzler and Rosenkranz 2007). Aside from problems in the observation operator, there are short-comings in the forecast model, which can lead to biases in the surface and near-surface fields. For instance, ECMWF presently employs a single-layer snow model, which will be unable to fully represent all thermal conditions of the real snow pack (e.g., Arduini et al. 2019). Furthermore, the atmospheric part of the ECMWF system currently does not represent snow over sea-ice, again giving rise to biases. An under-estimation of background errors over snow and sea-ice due to an under-spread Ensemble of Data Assimilations (EDA) further adds to the challenge (Lawrence et al. 2019b).

The purpose of the present memorandum is two-fold: Firstly, we will investigate the addition of 183 GHz humidity-sounding channels from ATMS over snow-covered areas. These channels are not presently assimilated in the ECMWF system, primarily due to concerns about the adequacy of forward-modelling the observations in these regions when ATMS was first introduced. However, adequate approaches have been developed for other sensors such as MHS, and these will be adopted here for ATMS. Secondly, we will investigate the effect of using a Lambertian rather than a specular assumption on the forward modelling of surface-sensitive MW radiances. This addresses one of the issues identified in modelling the observations, ie the suggestion that specular reflection is a poor assumption over snow-covered surfaces in the MW. Guedj et al. (2010), for instance, showed better agreement between observations and model equivalents for AMSU-A channels around 50 GHz when a Lambertian or semi-Lambertian assumption was used in the radiative transfer. The degree of Lambertianity appeared to be seasonally dependent, possibly reflecting different conditions of the snow pack. In the present memorandum we will extend this investigation to the 183 GHz humidity-sounding frequencies. We will also perform assimilation trials to identify the impact of a Lambertian treatment in global NWP. The extended use of ATMS observations over snow as well as the better forward modelling of MW observations over snow and sea-ice surfaces are part of the wider strategy towards an “all-surface” use of MW radiances in the ECMWF system.

The structure of the memorandum is as follows. First, the methods used to assimilate 183 GHz channels from ATMS over snow are introduced, as well as the approximation to represent Lambertian rather than specular reflection in the radiative transfer. Then, the effect of using a Lambertian assumption is assessed through background departure statistics for ATMS. This is followed by assimilation trials that evaluate separately the effect of adding 183 GHz humidity-sounding channels from ATMS over snow, as well as replacing the specular assumption in the radiative transfer with a Lambertian or semi-Lambertian one over snow and sea-ice for ATMS and AMSU-A. Finally, conclusions are summarised in the last section.

2 Methods

In the ECMWF system, ATMS is presently assimilated in clear-sky conditions only, and two ATMS instruments are currently used (S-NPP, NOAA-20). The initial assimilation settings and forecast impact are described in detail in Bormann et al (2013). Subsequent developments include the introduction of the assimilation of surface-sensitive channels over land (Lawrence and Bormann 2014), as well as an update of the assumed observation error, taking into account inter-channel error correlations (Weston and Bormann 2018). As ATMS has smaller footprints and hence larger sample noise than heritage sensors such as AMSU-A, 3x3 footprint averaging is employed prior to the assimilation of ATMS data.

2.1 Retrieval of emissivities over snow

The 183 GHz humidity sounding channels on ATMS are presently not assimilated over snow-covered land at ECMWF. To introduce the assimilation of these channels over snow, we adapt methods that have been developed for similar other sensors in the all-sky system. For the radiative transfer, the surface is described through an effective skin temperature taken to be the top-surface level from the forecast model, and an effective emissivity retrieved from a window channel observation which is otherwise not used in the assimilation. Following Karbou et al (2006), the surface emissivity retrieval is based on rearranging the simplified radiative transfer equation, and uses the background skin temperature as well as the atmospheric conditions from the background as input. The surface is assumed to be specular in the emissivity retrieval, as well as the radiative transfer for the assimilated sounding channels.

Over snow-covered land surfaces, the 150/157 GHz channel is used for MHS and SSMIS to retrieve the emissivity subsequently adopted for the assimilation of the 183 GHz channels, and a similar approach is adopted here for ATMS using the available 165 GHz channel. The choice of the emissivity retrieval channel is a trade-off between sufficient surface-sensitivity, to allow an accurate retrieval, and proximity in frequency to the assimilated sounding channels, to avoid errors due to spectral gradients neglected when the surface emissivity retrieved at one frequency is applied to another frequency. For snow-free land surfaces, emissivity variations with frequency are sufficiently small, so the 89/91 GHz channel is usually used for emissivity retrievals for 183 GHz sounding channels, as it offers better surface-sensitivity in clear-sky atmospheric conditions. In contrast, the alternative 150/165 GHz channel is less (or not at all) sensitive to the surface in moist atmospheres, rendering an emissivity retrieval impossible with this channel in these conditions. Over snow and sea-ice, however, spectral gradients in emissivity are much larger, so the use of the 89/91 GHz channel leads to larger errors. Di Tomaso and Bormann (2012) recognised, however, that over sea-ice, the 150/165 GHz channel can be used for the emissivity retrieval, as the atmosphere tends to be much drier and hence sufficiently transparent at this frequency. The approach has subsequently been extended to snow-covered land surfaces for sensors used in the all-sky system at ECMWF, ie SSMIS, MHS, and MWHS-2.

The above modifications are used to assimilate channels 20-22 of ATMS over snow, in line with choices for other MW sensors. To identify areas strongly affected by clouds or errors in the surface representation, any fields of view for which the absolute value of the departures in the lowest-peaking 183 GHz channel (channel 18) exceeds 2.5 K are rejected over snow. Snow-covered areas are identified here through the model's snow cover, combined with the requirement for the surface temperature to be below 278 K. The latter is a crude criterion, likely to also capture some scenes that are not covered by snow.

2.2 Lambertian effects

To account for Lambertian effects in the radiative transfer, we employ a parameterisation previously suggested by Mätzler (1987). This models the diffuse reflection by calculating the down-welling radiation with an effective zenith angle. This effective zenith angle is derived by integrating the down-welling contribution over a semi-sphere, assuming a homogeneous atmosphere. It is dependent on the zenith opacity, and for the channels considered here it varies typically between 40° for channels that are more weakly surface-sensitive and 56° for more strongly surface-sensitive channels. In contrast to previous work by Guedj et al (2010), who assumed a fixed effective zenith angle of 55°to model the Lambertian reflection, we account here for the zenith-opacity dependence of the effective zenith angle as given in Mätzler (1987). This was found to perform slightly better in comparisons between observations and background equivalents (Appendix A.2). A polynomial fit to the original equation is used for this pur-

pose to speed up the calculations (Appendix A.1). Compared to a specular assumption, the Lambertian effect will be largest where the effective zenith angle used for the down-welling radiation differs most from the actual satellite zenith angle, ie it will be largest close to nadir. In contrast, the effect will be smaller for conical scanners which typically have satellite zenith angles around 53°. The approximation used for Lambertian surface conditions is strictly only applicable to clear-sky or homogeneous conditions; using Lambertian surface reflection together with scattering radiative transfer is more complex, and it is left for future work.

In the following work, the Lambertian/specular assumption for the surface reflection is made for both the emissivity retrieval, as well as the subsequent radiative transfer calculations for the sounding channels. We will initially either assume that the surface is fully specular, or that it is fully Lambertian. Depending on the characteristics of the snow pack, a mixture between the two is possible, and this can be modelled by introducing a "specularity" parameter that specifies the weighting between the specular/Lambertian treatment of the down-welling radiation in the radiative transfer parameter. A specularity parameter of 1 indicates a specular surface, whereas a specularity parameter of 0 indicates fully Lambertian behaviour, with values in-between indicating mixtures between specular and Lambertian behaviour. Guedj et al (2010), for instance, found that Antarctica shows seasonal variations in the surface characteristics for observations near 50 GHz, with a fully Lambertian assumption working best over winter, whereas a semi-Lambertian or even specular assumption giving better results during summer.

3 Evaluation of Lambertian effects over snow and sea-ice

We will investigate the effect of modelling Lambertian surface reflection using the cross-track scanning ATMS instrument. It offers a good range of sounding channels in the 50-60 GHz and 183 GHz frequency bands. As it is assimilated using clear-sky radiative transfer in the ECMWF system, the choice of ATMS also avoids the complexities of treating a Lambertian surface with a scattering atmosphere. Nevertheless, findings about the relevance of Lambertian effects should be similarly applicable to an all-sky treatment of MW radiances, once a suitable parameterisation has been developed. We will employ Lambertian reflection only over snow- or sea-ice-covered surfaces, as determined by the forecast model; all other areas continue to assume specular reflection.

Lambertian effects will be investigated by comparing observations to model equivalents, calculated using the specular and the Lambertian surface assumption, respectively, with the same short-range forecasts as input. The latter are taken from assimilation experiments with a spatial model resolution of $T_{CO}399$ ($\approx$ 25 km), a final incremental analysis resolution of T_L 159 ($\approx$ 125 km), and 137 levels in the vertical, and they cover selected months in 2020. The assimilation experiments use the standard configuration of the ECMWF system, including using the specular assumption in the radiative transfer over land, and no assimilation of 183 GHz ATMS channels over snow. When considering statistics of differences between observations and short-range forecast equivalents (ie background departures), the usual bias corrections are applied, obtained through variational bias correction during the assimilation. As the radiative transfer in the assimilation experiment is using the specular assumption over land, the bias correction may partially reflect this. However, as the bias parameters are derived globally, and hence dominated by snow/ice-free areas, this effect is likely to be comparatively small. Our analysis is based on statistics derived using all observations and clear-sky radiative transfer, without screening for cloud. This is justified as over snow and sea-ice the contribution from clouds in the radiative transfer is typically small compared to the effects considered here, with mean differences between cloudy and clear simulations on average around an order of magnitude smaller than the signals investigated. Using all data in the statistics avoids comparisons between different sampling and masking of features through quality control.

3.1 Humidity sounding channels at 183 GHz

With the specular assumption, large scan-dependent biases are seen for the 183 GHz humidity-sounding channels over snow and sea-ice (e.g., Fig. 1a, b for the example month of January 2020). The bias reaches

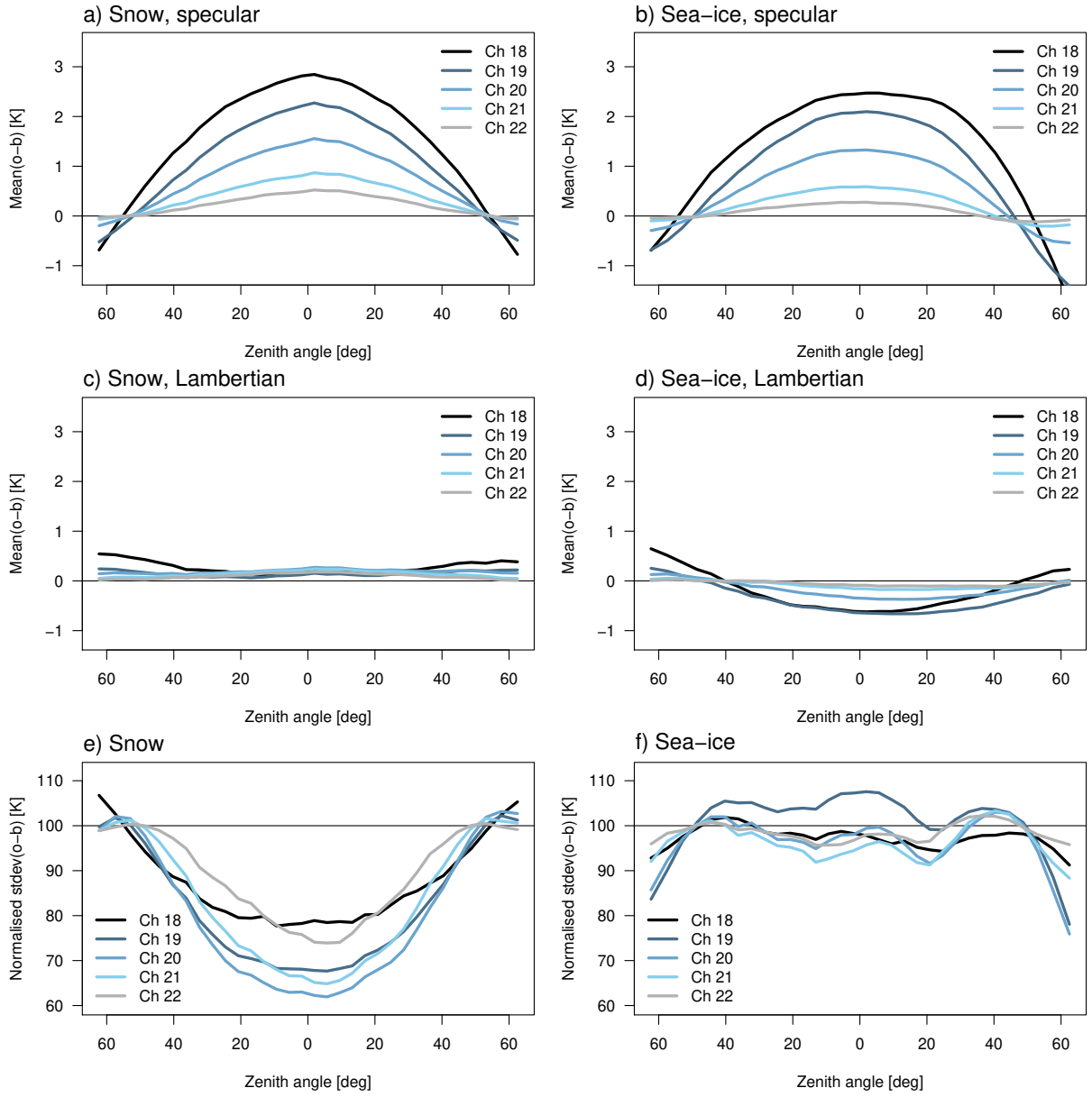

Figure 1: a) Mean departures (after bias correction) over snow-covered land surfaces as a function of scan-position for S-NPP ATMS channels 18 to 22 when the specular assumption is used. Statistics are for January 2020 using observations over the Northern Hemisphere only. The Figure is labelled on the x-axis with the average zenith angle per scan-position. Model values are used to determine snow-covered surfaces, and observations with a model orography higher than 1000 m are excluded. b) As a), but for sea-ice surfaces. c) As a), but using the Lambertian rather than the specular assumption. d) As d), but for sea-ice surfaces. e) As a), but for the standard deviation of background departures obtained using the Lambertian assumption, normalised by values obtained using the specular assumption [%]. f) As e), but for sea-ice surfaces.

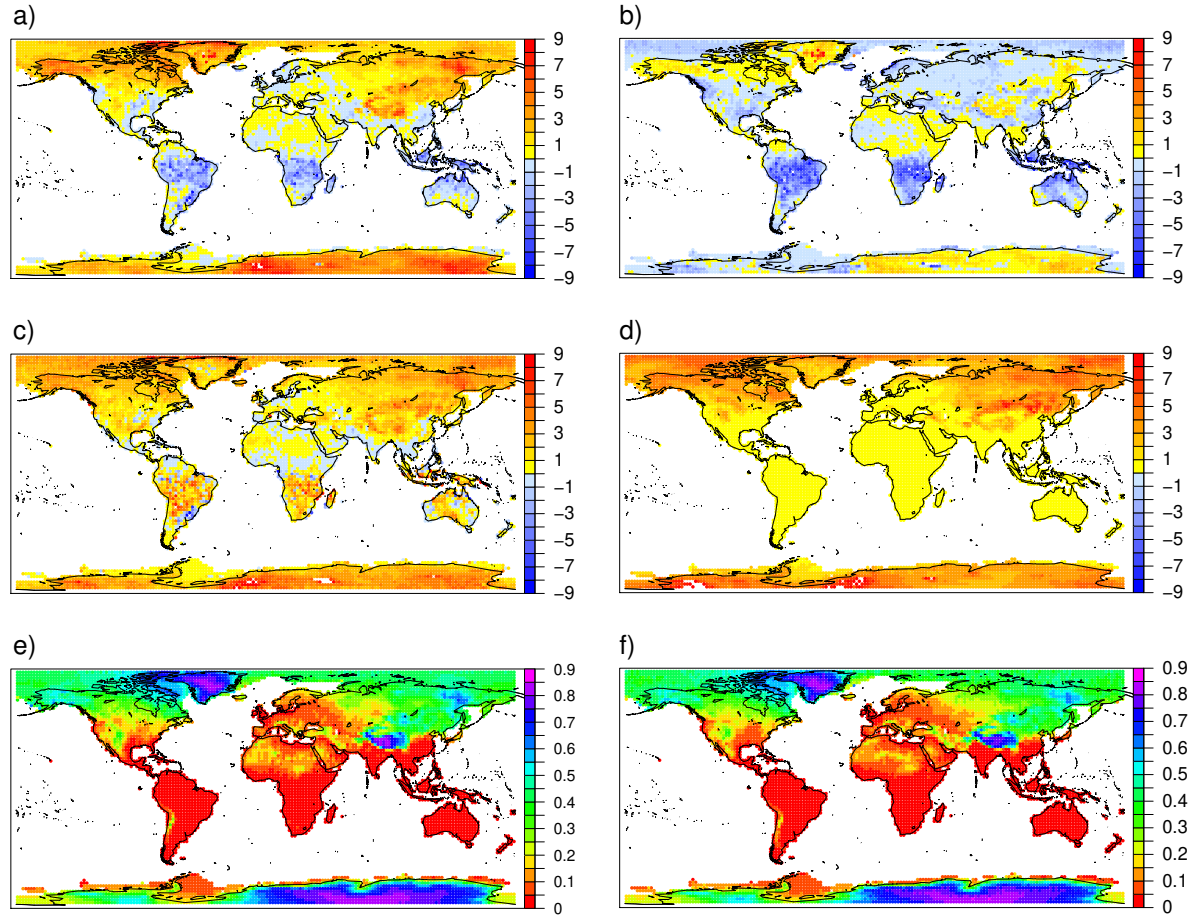

Figure 2: a) Map of mean observation minus background departures (after bias correction) [K] for S-NPP ATMS channel 19 for January 2020 for low zenith angles (ie $< 10°$). b) As a), but for S-NPP ATMS channel 18 for high zenith angels (ie $> 50°$). c) Difference between the biases shown in a) and b). d) As c), but calculated from differences between simulations from background values, in which the Lambertian and specular simulations have been used over snow-covered and sea-ice regions. Away from snow-covered and sea-ice regions, the specular assumption is used in both simulations and differences are hence close to zero. e) Map of the mean surface-to-space transmittance for S-NPP ATMS channel 19 for January 2017 for low zenith angles (ie $< 10°$). f) As e), but for S-NPP ATMS channel 18 for high zenith angels (ie $> 50°$).

3 K in the lowest-peaking channel (channel 18) at nadir for low zenith angles, which is significant given typical standard deviations of background departures for used data of around 1.2 K. Departures are close to unbiased for all channels for high zenith angles around 55°. A similar behaviour has been pointed out by Bormann et al (2017), and it is qualitatively consistent with characteristics expected due to neglected Lambertian effects. Indeed, when the Lambertian assumption is used in the radiative transfer simulations instead, biases are typically below 0.5 K regardless of scan-position/zenith angle (Fig. 1c, d). Furthermore, over snow-covered land, there is a clear reduction of the standard deviation of background departures for all channels, with the largest reductions exceeding 35% for channel 20 at nadir (Fig. 1e). This suggests that assuming a Lambertian surface addresses not only a general bias, but also accounts for some of the situation-dependent variation in the radiative transfer. In contrast, over sea-ice, there is a small increase in the standard deviation of background departures around nadir for channel 19, though little change for other channels (Fig. 1f). The slight increase may suggest that a fully Lambertian surface

assumption is not optimal, or that other, possibly previously compensated errors contribute.

Figure 2a-c explores the geographical variation of the differences in the observed bias between low and high zenith angles when the specular assumption is used. As seen in Fig. 1, these differences are a measure of the size of the Lambertian effect. Fig. 2a shows a map of the bias in channel 19 for low zenith angles, with large positive biases visible over snow-covered surfaces. The negative biases in the tropics are due to neglected clouds in the radiative transfer and are not relevant for our discussion here. For comparison, Fig. 2b shows a map of biases for channel 18 at high zenith angles, for which Lambertian effects matter less. Here, biases are mostly staying between ± 1 K over the high latitude regions. Due to the larger atmospheric paths at higher zenith angles, any given channel will show less surface-sensitivity at higher zenith angles, and if there are other surface-related biases present (e.g., in the skin-temperature used), this would result in a weaker effect at high zenith angles if the same channel was considered. To compensate for this effect, Fig. 2b shows statistics for the lower-peaking channel 18, which at high zenith angles has a similar surface-sensitivity as channel 19 at low zenith angles (cf Fig. 2e, f). The difference between the two biases is shown in Fig. 2c, illustrating further the geographical variation of the viewing-angle-dependent biases. In comparison, Fig. 2d shows the same quantity, but derived from differences between radiative transfer simulations with Lambertian vs the specular assumption over snow or sea-ice. It is apparent that the simulations shown in Fig. 2d can explain most of the geographical features in bias associated with snow and sea-ice apparent in Fig. 2c. This is consistent with the finding that standard deviations of background departures are reduced over snow when the Lambertian assumption is adopted, and further indication that treating the surface as Lambertian allows better forward-modelling of the observed radiances. Note that the results shown provide little indication that the skin-temperature introduces a significant bias for these 183-GHz channels, as biases in the background departures for channel 18 are fairly low over snow/sea-ice regions (Fig. 2b) despite strong surface-sensitivity.

To further highlight the relationship between the observed and simulated biases and to explore seasonal variations, Fig. 3 shows scatter plots of the quantities shown in Fig. 2c and Fig. 2d for different months, separately for both hemispheres. Here, each point in the scatter plot represents statistics for a geographical area of equal-size of approximately 111 km $\times$111 km that has sea-ice or snow-cover during the month of January 2020. As can be seen, there is a good correspondence around the diagonal line between the observed bias and the simulated bias that we would expect when the specular assumption is used and the surface in reality shows Lambertian behaviour. There is some indication that a slope of less than one (e.g., 0.8) would provide a better fit, translating to a specularity parameter of around 0.2. While some scatter is present, particularly for the Southern Hemisphere, the relationship overall appears broadly similar for the different months and different hemispheric regions shown, with no clear indication of seasonal dependence. This is different from the findings of Guedj et al (2010) for observations around 50 GHz. They found that a fully Lambertian assumption works best over winter, whereas a semi-Lambertian or even specular assumption gave best results during summer, and hypothesised that this is related to the prevalence of dry vs wet snow over the different seasons. The different findings for 183 GHz observations are likely a result of the higher frequencies and hence different sensitivities to the consistency of the snow pack.

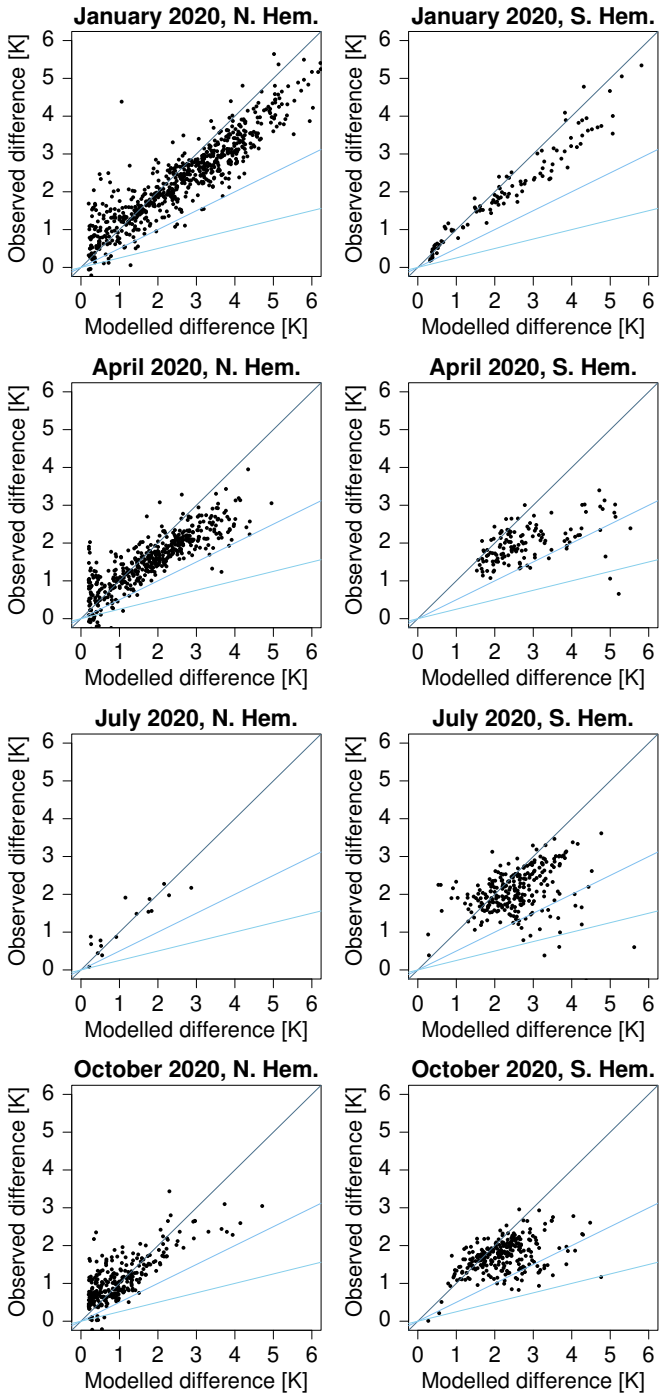

Figure 3: Scatter plots of the following quantities derived for snow or sea-ice covered equal-area regions for the months indicated in the title: y-axis: difference between the observed bias in channel 19 at low (<10°) zenith angles and the observed bias in channel 18 at high (>50°) zenith angles; x-axis: difference between Lambertian and specular simulations for channel 19 at low zenith angles minus differences between Lambertian and specular simulations for channel 18 at high zenith angles. The two columns show separately statistics for the Northern (left) and Southern (right) Hemisphere, with the four rows showing results for different months of the year 2020. Points with a model orography greater than 2000 m are excluded.

3.2 Temperature sounding channels near 50 GHz

Similar to the results for the humidity-sounding channels, the 50 GHz temperature-sounding channels of ATMS also show clear scan-dependent biases over snow and sea-ice when the specular assumption is used (Fig. 4a,b). The biases are much reduced when the surface is assumed to be Lambertian instead (Fig. 4c,d), consistent with results previously found by Guedj et al. (2010) or Bormann et al. (2017). However, residual biases are still notable for several channels, including a bias of around 0.5 K at nadir for channel 6, the lowest temperature-sounding channel considered for assimilation. This is significant compared to the standard deviation of background departures for this channel (0.2-0.6 K), and this may point to the presence of other bias sources in the background departures. There is also indication of

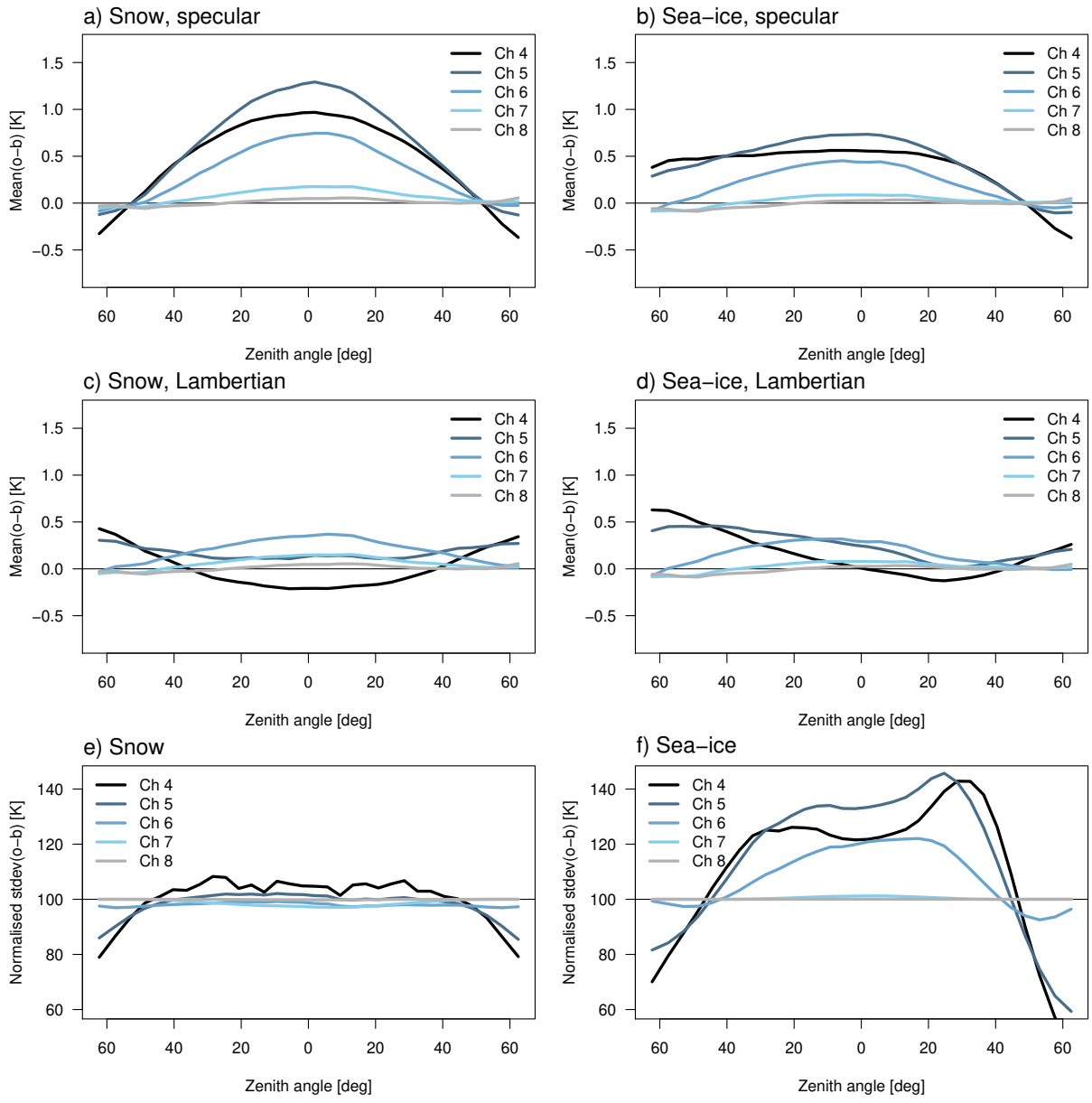

Figure 4: As Fig. 1, but for the S-NPP ATMS channels 4-8.

over-correction with negative biases at nadir for channel 4, which suggests that a partial Lambertian assumption may overall be more appropriate. Note that the slight asymmetry in the bias visible in the statistics over sea-ice is the result of different geographical sampling due to the satellite's inclination, with the lower scan-positions (left hand side of the plot) sampling more coastal areas, and the higher scan-positions (right hand side of the plot) sampling primarily areas near the pole. Using the Lambertian assumption also leads to poorer standard deviations of background departures for lower zenith angles over sea-ice (Fig. 4e,f). This may be an indication that a fully Lambertian surface assumption is not optimal, or again that other error sources play a significant role.

A less consistent relationship for the 50 GHz channels is also seen when comparing observed bias differences with those expected from simulations of the Lambertian effect for different months of the year (Fig. 5). These Figures have been produced in the same way as Fig. 3, but this time taking the difference between biases in channel 5 at low zenith angles and biases in channel 4 at high zenith angles as a measure of Lambertian-like effects. While there is some relationship between the observed bias differences and the ones expected from using a specular assumption when the surface is actually Lambertian, there appears to be more variation in the slope of the relationship. The statistics suggest that a fully Lambertian assumption may be appropriate for January over the Northern Hemisphere, whereas the statistics for July over the Southern Hemisphere or for April over the Northern Hemisphere suggest that a semi-Lambertian behaviour may be more appropriate. The latter can be estimated from alternative slopes plotted in the graph. The behaviour is thus more complex than what we found for the 183 GHz channels, for which the observed biases more consistently suggest near-Lambertian surface characteristics (cf Fig. 5).

The finding that the degree of specularity for 50 GHz may be dependent on the season likely reflects different states or consistencies of the snow pack, for instance linked to the presence of new snow. The finding is similar to results by Guedj et al (2010). However, considering data over Antarctica, they found that a fully Lambertian assumption was best during winter, whereas a semi-Lambertian or even specular assumption appeared to give best results during summer. While there is some indication of similar behaviour in our results for the Northern Hemisphere, no such agreement is apparent for the statistics over the Southern Hemisphere for which a semi-Lambertian behaviour appears more appropriate for the four months shown. Further investigations suggest that scenes with a higher scatter index between the 24 and 89 GHz channels appear to follow a more Lambertian behaviour (not shown). With higher scatter indices being indicative of new snow with finer ice-crystals, such correlation appears physically plausible. Rosenkranz and Mätzler (2008) found some relationship between the degree of Lambertianity for 50-GHz channels and a 37-GHz reflectivity-polarisation index from SSMI. Using such indicators, it may be possible to estimate the expected degree of specularity, but this is left for future work.

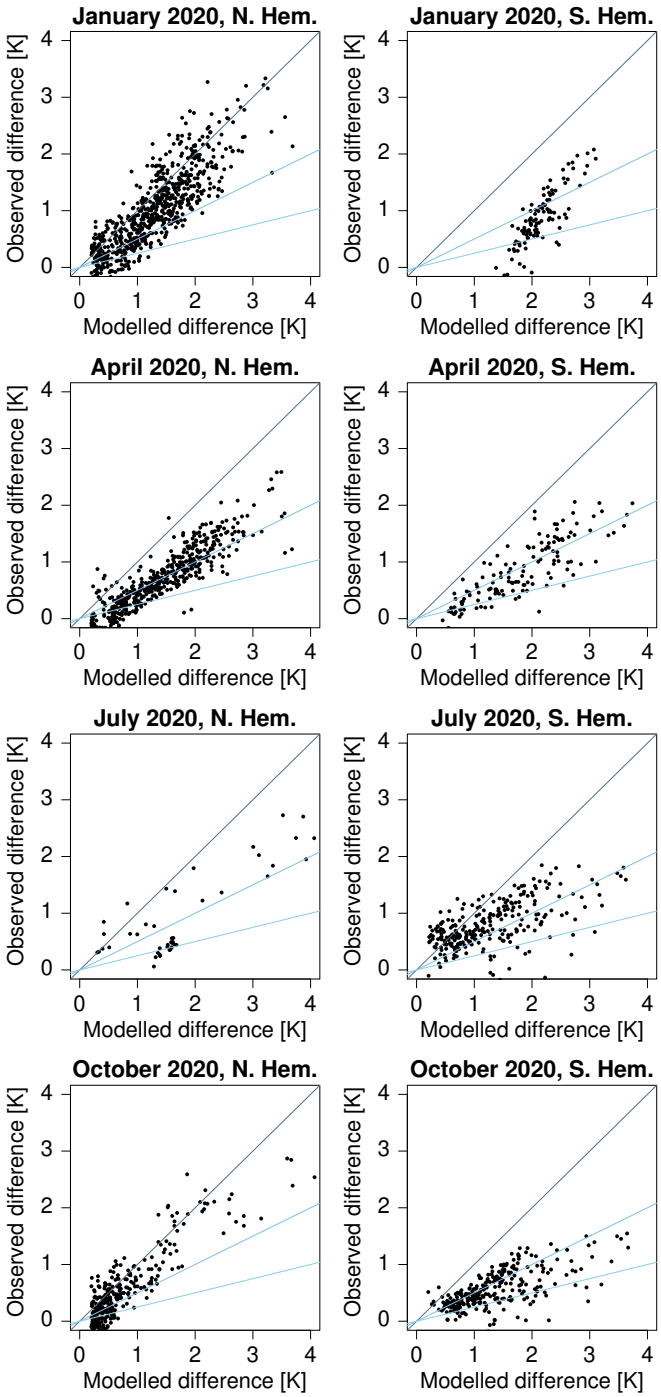

Figure 5: Scatter plots of the following quantities derived for snow or sea-ice covered equal-area regions for the months indicated in the title: y-axis: difference between the observed bias in channel 6 at low (<10°) zenith angles and the observed bias in channel 5 at high (>50°) zenith angles; x-axis: difference between Lambertian and specular simulations for channel 6 at low zenith angles minus differences between Lambertian and specular simulations for channel 5 at high zenith angles. The two columns show separately statistics for the Northern (left) and Southern (right) Hemisphere, with the four rows showing results for different months of the year 2020. Points with a model orography greater than 2000 m are excluded.

3.3 Effect on the retrieved emissivities

The statistics presented above consider the Lambertian effect in the simplified radiative transfer equation used for both the emissivity retrieval as well as the forward calculations for all channels. As can be expected, assuming Lambertian reflection has a considerable effect on the retrieved emissivities, as illustrated in Fig. 6. For snow, the average retrieved emissivities are more constant with scan-position when the Lambertian assumption is used than in the specular case. This is true for the 50 GHz emissivity retrieval as well as the 165 GHz emissivity retrieval. A scan-position-dependence in the emissivity for the cross-track scanning ATMS instrument either indicates a difference in the emissivity for different polarisation (as the channel polarisation changes with scan-position) or a viewing-angle dependence. Depending on the conditions, both may be less likely for snow, so the more constant result appears more plausible here. However, any biases in the effective skin temperature used in the retrieval will also affect the scan-dependence of the retrieved emissivities. As these cannot be ruled out, particularly for the 50-GHz channels, the interpretation of this finding is not clear. Over sea-ice, there is also a considerable change in the retrieved emissivity, but the main feature is an asymmetry in the retrieved emissivities for both the specular as well as the Lambertian case (Fig. 6b). These statistics are again affected by geographical sampling, with the higher scan-positions (right-hand-side of the plot) sampling more regions with multi-year ice which tends to show lower emissivities. It is hence not clear which of the two emissivity retrievals appear more reasonable.

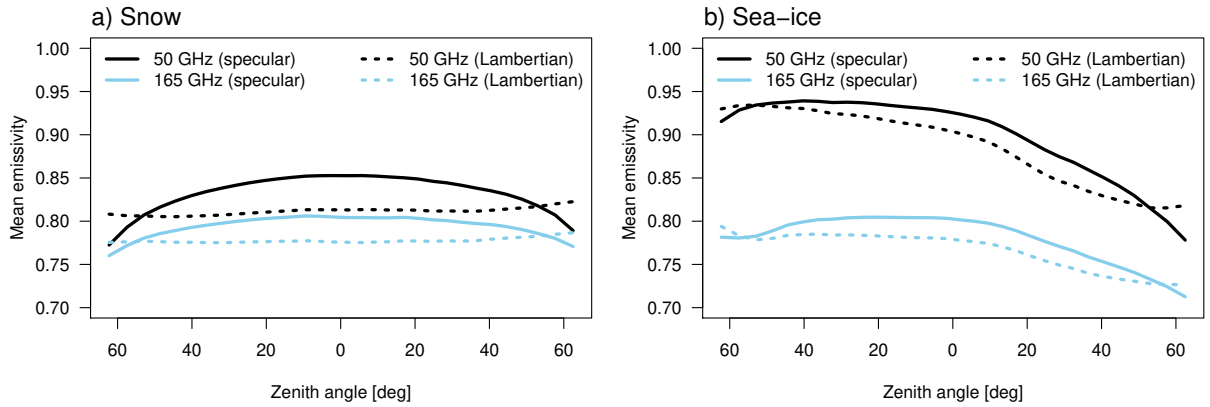

Figure 6: Mean retrieved emissivity at 50 GHz (black) and at 165 GHz (blue) as a function of scan position when the specular assumption is used (solid lines) compared to using the Lambertian assumption (dashed lines). Statistics are shown for snow-covered land surfaces (a) and sea-ice areas (b), and they are based on Northern Hemisphere observations in January 2020, as described in Fig. 1. The Figure is labelled on the x-axis with the average zenith angle per scan-position.

4 Assimilation trials

We will now summarise results from assimilation trials that assess the use of ATMS over snow and sea-ice using a Lambertian assumption. The objective of this is two-fold. Firstly, we assess the introduction of the higher-peaking 183 GHz channels of ATMS over snow; this brings the usage of the ATMS humidity channels in line with that of other sensors with similar 183 GHz channels. Secondly, we investigate the change from using a specular assumption for the surface characteristics in the radiative transfer calculations to assuming Lambertian or partial Lambertian reflection. A Lambertian parameterisation

is presently only available for the clear-sky version of RTTOV, so experimentation with this will be confined to instruments used in the clear-sky system, namely ATMS and AMSU-A. Three assimilation experiments are used here:

Control: An experiment that uses observations in a similar way as the present operational ECMWF system. The usage of surface-sensitive MW sounding channels is as described in Bormann et al (2017) with updates summarised in Weston et al (2017), and an overview of the channel usage is given in Table 1. As can be seen, the majority of channels is used over all surface conditions, but for some channels the usage is more restricted for the lowest-peaking channels, particularly over snow and sea-ice.

AtmsSnow: As Control, but ATMS channels 20-22 are added over snow. The lowest humidity-sounding channels 18 and 19 are not activated, as these exhibit very strong surface-sensitivity during the dry polar winters, with a surface-to-space transmittance well over 0.3 on many occasions. Channel

Table 1: Usage of the lower-peaking microwave sounding channels in the Control experiment.

Type	Instruments and clear-sky/all-sky	Frequency [GHz]	Snow-free land	Snow-covered land	Sea-ice
T	AMSU-A, clear-sky	53.596±0.115	yes[1]	yes[1]	N.Hem. only
		54.4	yes[2]	yes[2]	yes
		54.94	yes	yes	yes
	ATMS, clear-sky	53.596±0.115	yes[3]	yes[3]	no
		54.4	yes[4]	yes[4]	yes
		54.94	yes	yes	yes
	MWHS-2, all-sky	118.75 ±2.5	no	no	no
		118.75 ±1.1	yes[7]	yes	no
		118.75 ±0.8	yes[7]	yes	no
q	ATMS, clear-sky	183.31 ±7	yes[5]	no	no
		183.31 ±4.5	yes[5]	no	no
		183.31 ±3	yes[6]	no	yes
		183.31 ±1.8	yes[6]	no	yes
		183.31 ±1	yes[7]	no	yes
	MHS, MWHS-2, SSMIS, all-sky (not all channels are available on all instruments)	183.31 ±7/190.311	yes[5]	no	no
		183.31 ±4.5	yes[5]	no	no
		183.31 ±3	yes[6]	yes	yes
		183.31 ±1.8	yes[6]	yes[6]	yes
		183.31 ±1	yes[7]	yes[7]	yes

[1] Except over Antarctica.
[2] Except where orography is higher than 1500 m over Antarctica.
[3] Except where orography is higher than 500 m (1000 m in the tropics).
[4] Except where orography is higher than 1500 m (2000 m in the tropics).
[5] Except where orography is higher than 800 m.
[6] Except where orography is higher than 1000 m.
[7] Except where orography is higher than 1500 m.
[8] Except for latitudes poleward of ±60°.

18 departures are used for quality-control over snow and sea-ice, and locations where the absolute value of the background departure in channel 18 exceeds 2.5 K are rejected. This is aimed to address potential cloud contamination or poor surface treatment. The specular assumption is used in all radiative transfer calculations over land or sea-ice.

AtmsSnowLambert: As AtmsSnow, but using Lambertian reflection over snow and sea-ice regions. For the ATMS channels at 165.5 GHz and above, we treat the surface as fully Lambertian, whereas for all other ATMS channels a semi-Lambertian behaviour is used. The choices for the degree of Lambertianity were motivated by the monitoring results presented earlier. While the monitoring results suggest that some variations may be appropriate, especially for the 50-GHz channels, there are neglected here for now. The Lambertian/semi-Lambertian assumption is used in the emissivity retrieval as well as any subsequent radiative transfer calculations.

The experiments are performed over the periods 20 June – 30 September 2019 and 1 December 2019 – 31 March 2020, covering a little over 7 months in total. The experiments use ECMWF's 12-hour 4D-Var system with a model resolution of T_{CO} 399 (approximately 25 km), a final incremental analysis resolution of T_L 159 (approximately 125 km), and 137 levels in the vertical.

4.1 Changed ATMS and AMSU-A usage

The modifications in AtmsSnow and AtmsSnowLamb lead to a considerable increase in the number of assimilated observations for the affected humidity-sounding channels, as highlighted in Fig. 7 for channel 20. Channel 20 is representative of the other ATMS humidity-sounding channels activated over snow in AtmsSnow, and the activation adds the expected coverage over large areas over land at higher latitudes in winter (cf Fig. 7a and b). A smaller, but still notable increase in the number of assimilated observations results from the Lambertian surface treatment over snow and sea-ice for the 183 GHz channels, for instance over Canada or North-Eastern Siberia (cf Fig. 7b and c). This is a result of the smaller viewing angle-dependent biases, in combination with the quality control on background departures of the lowest-peaking 183 GHz channel to screen for errors in the surface description and cloud contamination. Figure 8a illustrates the interplay of this quality control and the zenith-angle dependent biases. For the AtmsSnow experiment (blue contours), many near-nadir views are rejected as the departures fall outside

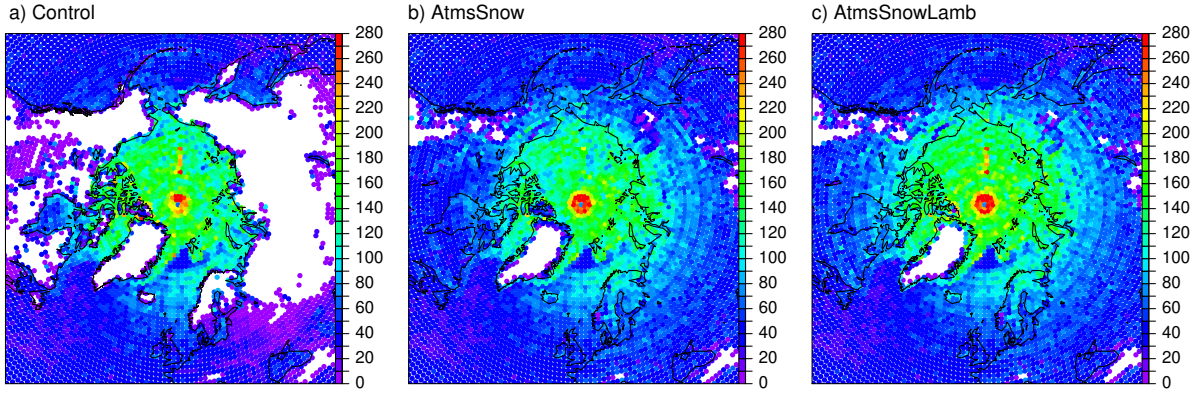

Figure 7: Map of the number of used observations in S-NPP ATMS channel 20 for February 2020 for the Control (a), the AtmsSnow (b) and the AtmsSnowLamb (c) experiment. The numbers are given per regions of approximately $111 \times 111 km^2$.

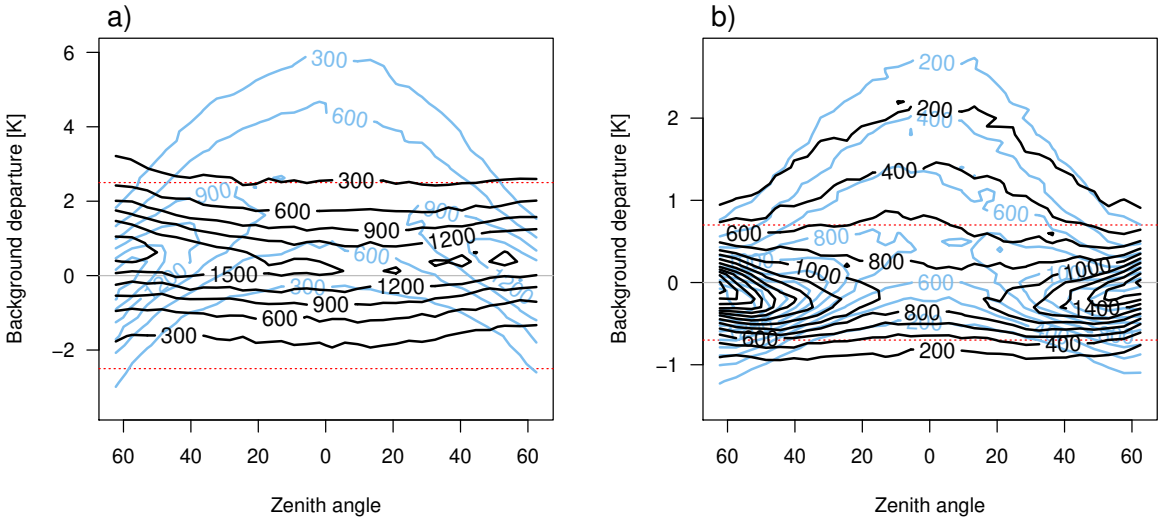

Figure 8: a) Histograms of background departures by scan-position for channel 18 observations of the S-NPP ATMS over snow. Statistics are shown for all data after bias correction, with a histogram interval of 0.25 K. Blue contours show histograms for experiment AtmsSnow with the specular assumption; black contours show values for AtmsSnowLamb using the Lambertian assumption. Red dashed lines indicate the threshold used for quality control on the absolute value of the background departures. b) As a), but for channel 5 and a histogram interval of 0.1 K.

the thresholds applied to the departure check for the lowest-peaking 183 Ghz channel, whereas this situation is much improved in the AtmsSnowLamb experiment (black contours). The result is an increase in the number of used observations for lower zenith angles (e.g., Fig. 9a, b). Note that the spatial thinning also affects the shape of the number of used observations by scan-position, as near-nadir scan-positions are closer to each other, so more observations are thinned out. For sea-ice, the asymmetric behaviour in the sampling seen in Fig. 9b is again due to the orbital inclination combined with the positioning of landmasses, leading to fewer observations with scan-positions on the left-hand-side of the graph observing sea-ice conditions. The overall increase in the number of assimilated humidity-sounding channels over the Northern Hemisphere during the winter period is around 30 % in AtmsSnow, with another 10 % added in AtmsSnowLamb. The number of observations used over snow-covered areas in AtmsSnowLamb now largely matches that over sea at similar latitudes, with the exception of Greenland or other regions with high orography which continue to be excluded to avoid larger errors due to elevated surface-sensitivity.

The improvements in the forward modelling of the 183 GHz channels when Lambertian reflection is assumed are also further highlighted in Fig. 10. As can be seen, biases in background departures (after bias correction) are mostly closer to zero over snow for channel 20 of ATMS, the lowest channel considered for assimilation over snow and sea-ice (cf Fig. 10a and b). Over sea-ice, there are some indications of an increased local negative bias in AtmsSnowLamb, possibly indicative of skin-temperature errors or regions where a fully Lambertian assumption is sub-optimal. The effect is, however, comparatively small. Given the locally different bias characteristics, there are also some minor adjustments to the variational bias correction. But since the bias models are constrained globally, these local changes in the mean bias correction are only of the order of a view hundreds of K, and thus more than a magnitude smaller than typical standard deviations of background departures. Standard deviations of background departures are reduced substantially, particularly for channel 20 for which reductions reach 55 % (Fig. 10c). This of course partially reflects a reduction of viewing-angle dependent biases. The statistics shown in Fig. 10 are for all observations before applying quality control to enable comparisons for a consistent sample.

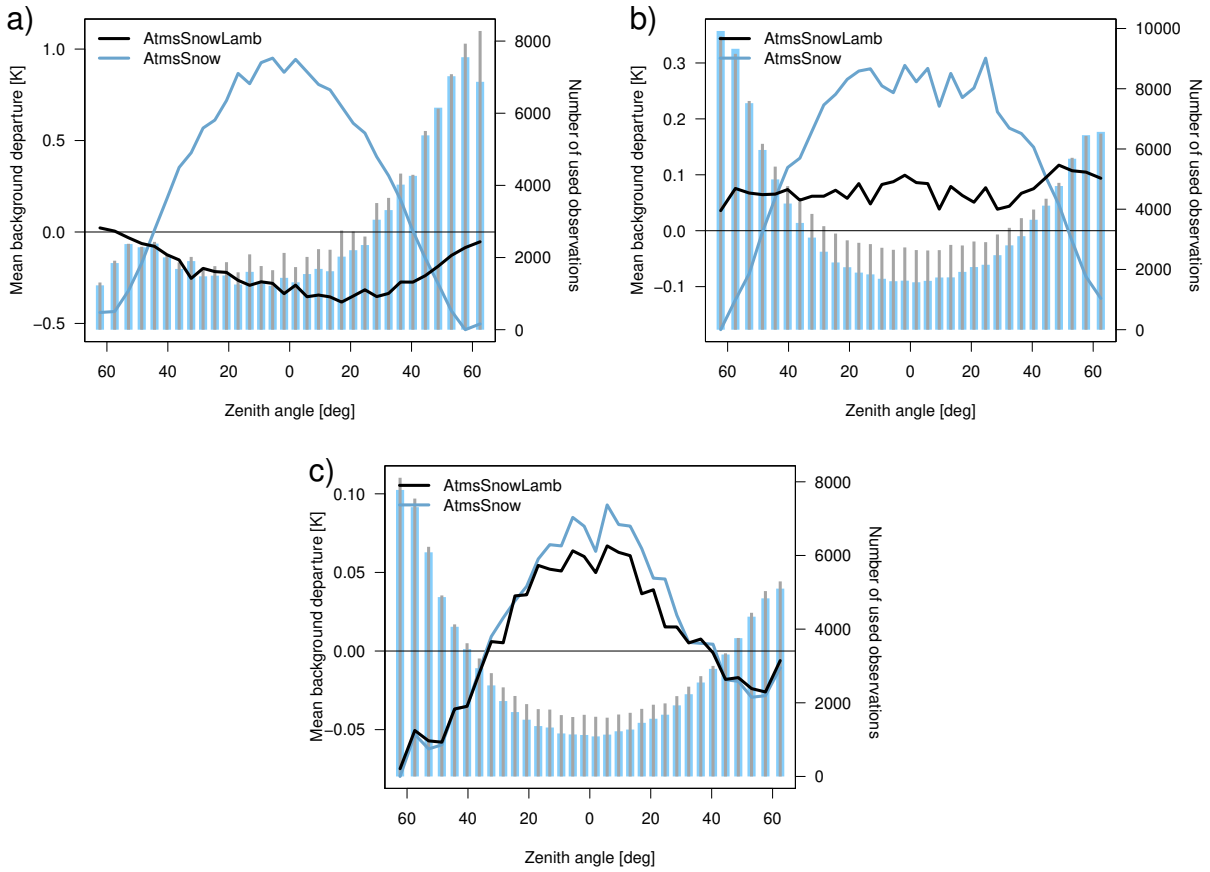

Figure 9: a) Mean background departures (after bias correction) for used S-NPP ATMS channel 20 observations over sea-ice as a function of scan-position, for the AtmsSnow experiment (blue) as well as the AtmsSnowLamb experiment (black). Also shown are histograms of the number of used observations (right x-axis). The Figure is labelled on the x-axis with the average zenith angle per scan-position. b) As a), but for data over snow. c) As b), but for channel 6.

The quality control for the 183 GHz channels means that some of the observations with the largest errors due to the specular assumption were previously discarded, thus limiting the potentially detrimental effect in the assimilation (e.g., Fig. 9a and b). After quality control, the standard deviation of background departures over snow and sea-ice is now mostly below 1 K for channel 20, and hence smaller than over some regions over sea, with absolute biases less than 0.5 K (not shown).

The usage of the lowest assimilated ATMS and AMSU-A temperature-sounding channel also changes as a result of the semi-Lambertian surface-treatment introduced in AtmsSnowLamb, though the changes are not as large as for the humidity-sounding channels. Biases in background departures (after bias correction) for all data are slightly reduced for channel 6 of ATMS, albeit mostly by only 0.1-0.2 K compared to bias values that locally reach 0.5-1 K (cf Fig. 11a and b). While this could indicate that locally the surface characteristics are more Lambertian than the semi-Lambertian treatment shown here, further investigations suggest that biases in the effective skin temperature used are likely to be a significant factor. Penetration depths differ between 50 and 183 GHz channels, a likely explanation why results in this respect differ from the ones for 183 GHz channels. Standard deviations of background departures for channel 6 are reduced by up to 25 % over snow and sea-ice (Fig. 11c), again reflecting the better mod-

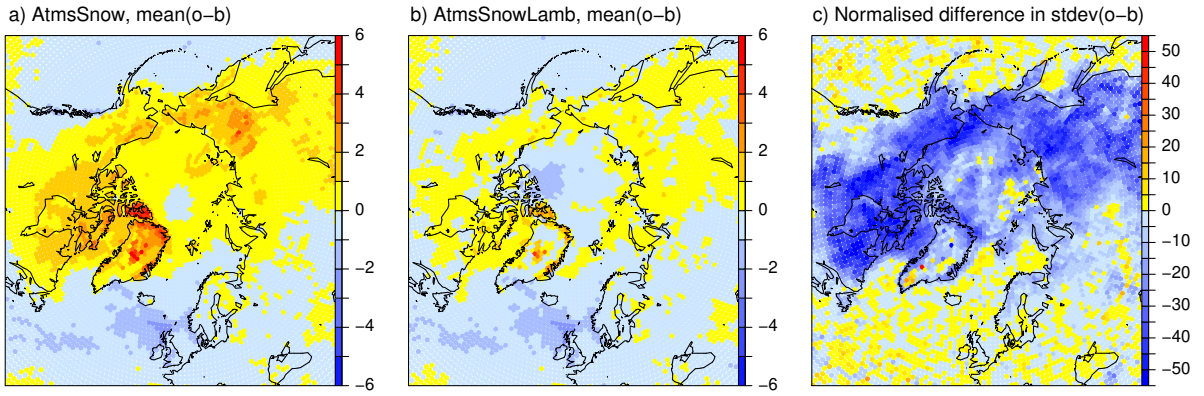

Figure 10: a) Map of mean background departures [K] for S-NPP ATMS channel 20 (after bias correction) for the AtmsSnow experiment. b) As a), but for the AtmsSnowLamb experiment. c) Map of normalised change in the standard deviation [%] in the AtmsSnowLamb experiment relative to the AtmsSnow experiment for S-NPP ATMS channel 20. For all three panels statistics are calculated for February 2020 for all observations.

elling of viewing-dependent biases as outlined in section 3. The improvements in the forward modelling of the 50 Ghz-channels leads to a small increase in the number of used observations (Fig. 12) The Figure shows the number of used observations for channel 7 are shown here, as channel 6 is not assimilated over sea-ice, but the channel 7 usage is otherwise similar to that of channel 6. For the Northern Hemisphere winter experiment, this amounts to an overall increase of 5-8 % for channels 6-8. Note that statistics shown in Fig. 11 are again for all observations, ensuring a consistent sample. The quality control applied to these channels includes a check on the background departures in the 52.8 GHz window channel, and this considerably affects the statistics for the sample of used observations (e.g., Figures 8b and 9c). Note that the lowest temperature-sounding channel of ATMS is not assimilated over sea-ice (in contrast to the assimilation of channel 5 for AMSU-A). During the course of this study, we investigated whether using the semi-Lambertian surface treatment permits a beneficial assimilation of ATMS channel 6 over sea-ice, but this was found not to be the case. It is likely that other issues such as biases in the used skin temperature continue to play a significant role here.

While we focused here on the statistics for ATMS, the improved forward-modelling for the lowest as-

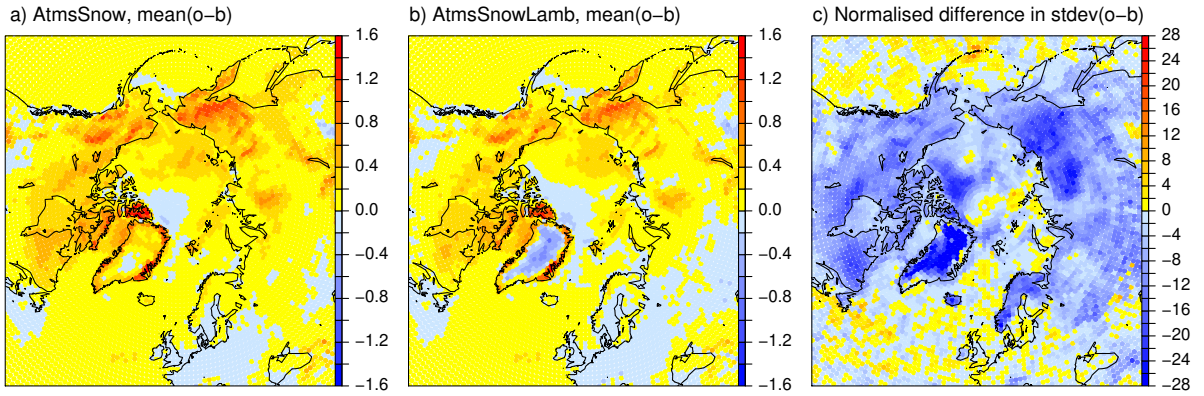

Figure 11: As Fig. 10, but for S-NPP ATMS channel 6.

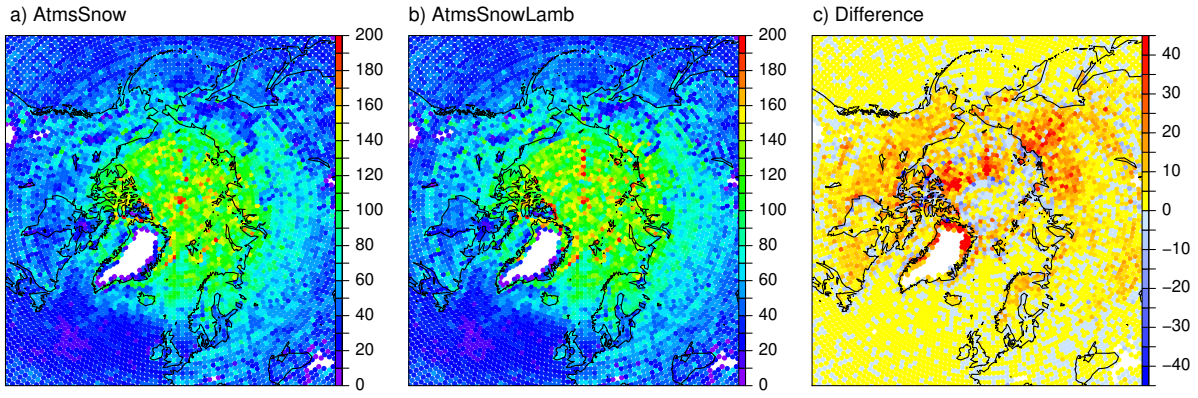

Figure 12: Map of the number of used observations in S-NPP ATMS channel 7 for February 2020 for the AtmsSnow (a) and the AtmsSnowLamb (b) experiment, as well as the difference between both (c). The numbers are given per regions of approximately $111 \times 111 km^2$.

similated temperature-sounding channel for all data is also reflected in statistics for AMSU-A, though the increase in the number of assimilated observations is much smaller (around 1 % over the Northern Hemisphere in winter). This is partly because of differences in the quality control applied to AMSU-A and ATMS. In addition to rejecting observations with too large absolute values of background departures in the 52.8 GHz channel, observations are also rejected for AMSU-A when the situation-dependent component of the observation error model becomes dominant (Lawrence et al. 2015). Such a check is presently not applied to ATMS. Aspects of the AMSU-A observation error model and quality control could be revisited to better reflect the altered departure characteristics.

While we focused here mainly on the Arctic region during winter, many of the aspects are also replicated for the South polar region during the Southern Hemisphere winter season. Note, however that due to the high altitude of the Antarctic Plateau the humidity-sounding channels and many of the lower-peaking ATMS channels remain excluded in this area due to the strong surface-sensitivity. The present developments may contribute to relaxing this restrictive use in the future.

4.1.1 Effect on skin-temperature estimation

Treating the surface as Lambertian or semi-Lambertian reflector has an effect on the skin-temperature retrieved as a sink-variable during 4D-Var. Figure 13a shows, for instance, a much weaker viewing-angle dependence in the mean skin-temperature increments for ATMS over Northern Hemisphere sea-ice in February 2020, with a clear reduction in the absolute magnitude of the increments. The response of the skin-temperature sink-variable is largely dominated by the background departure in the channel with the strongest surface-sensitivity which depends on meteorological conditions as well as quality control decisions. During the dry winter months over sea-ice, channel 20 tends to be the most surface-sensitive channel assimilated for ATMS. Comparison to Fig. 9a shows that the mean skin-temperature increment hence largely follows the mean background departures of channel 20 used in this region. Over snow-covered land surfaces, channel 6 instead tends to be the most surface-sensitive channel, and a similar pattern emerges here for mean skin-temperature increments and background departures (cf Figures 13b and 9c).

The findings illustrate how some of the biases arising from the specular assumption are currently aliased

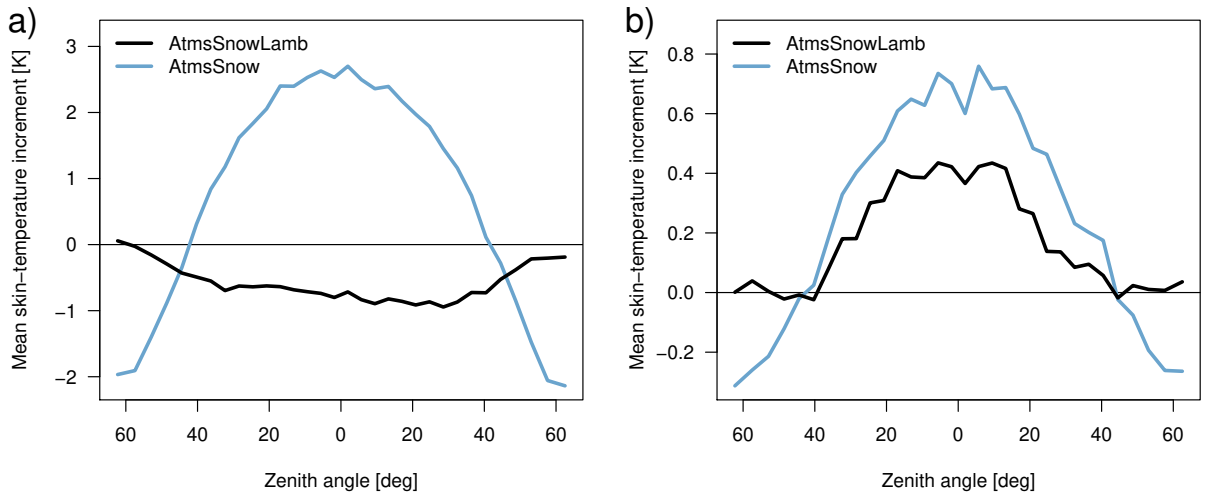

Figure 13: a) Mean skin-temperature increment over Northern Hemisphere sea-ice as a function of scan-position for S-NPP ATMS for used observations in February 2020. Black shows results for the AtmsSnowLamb experiment, whereas blue indicates results for the AtmsSnow experiment. The Figure is labelled on the x-axis with the average zenith angle per scan-position. b) As a), but for snow-covered land areas over the Northern Hemisphere.

into skin-temperature increments, and together with the quality control applied this protects the analysis in the Control from these biases. The findings have some implications for developments of different skin-temperature treatments in the ECMWF system. Efforts are presently underway to replace the field-of-view specific skin temperature sink variable with consistent multi-sensor skin-temperature analyses via an augmented control variable field (Massart et al. 2021). In this new approach, all sensors use the same hourly skin-temperature fields, and skin temperature is interpolated to the applicable location of the observations. To achieve this consistency, it is clearly important to reduce other errors that are currently aliased into the skin-temperature sink variable. This is includes the viewing-angle dependent forward-modelling biases investigated here.

4.2 Forecast impact

We will now summarise the forecast impact from adding the ATMS humidity-sounding channels over snow as well as the move to a Lambertian surface treatment over snow and sea-ice.

As expected, the impact from both changes investigated here is primarily confined to the higher latitudes where most of the snow and sea-ice are located, and it is most prominent during the winter months on each hemisphere (e.g., Fig.14). Adding the 183 GHz channels from ATMS over snow shows a notable improvement in verification against own analyses over the winter pole up to the day 1-forecast (e.g., Fig.14a and b), indicating an overall better consistency that is also visible in significantly reduced increments in this area (not shown). The Lambertian surface modelling gives a further small positive impact, with some statistically significant benefits lasting out to day 3 in the Antarctic region (e.g., Fig.14g). Similar signals are also present in other atmospheric variables. Verification against own analyses shows a particularly strong signal for lower tropospheric relative humidity over the polar regions during the respective winter months (Fig. 15). This is, however, largely an artifact of own-analysis verification, due to a significant dry model bias in the polar region during the respective winter months. This dry bias is very apparent in comparisons between radiosonde data and model fields (Fig. 16), showing a consider-

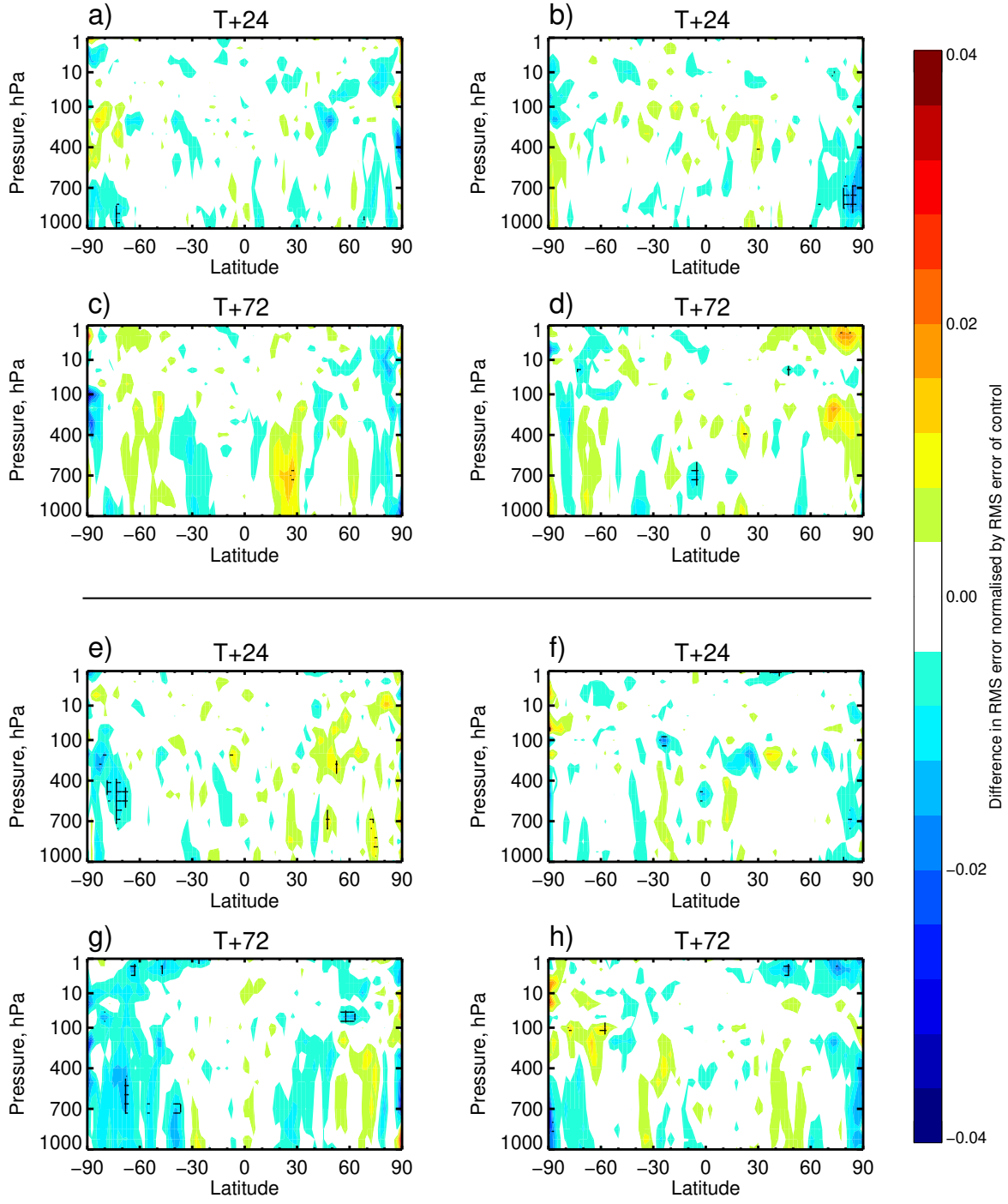

Figure 14: a) Zonal mean of the normalised difference in the day-1 root-mean-squared vector wind error between the AtmsSnow and the Control experiment for the 20 June – 30 September 2019 period. Negative values (blue) depict an improvement over the Control, with cross-hatching indicating statistical significance at the 95 % level. Each experiment has been verified against its own analysis. b) As a), but for the December 2019 – March 2020 period. c) As a), but for the day-3 forecast. d) As b), but for the day-3 forecast. e) As a), but for normalised difference in the day-1 root-mean-squared vector wind error between AtmsSnowLamb and AtmsSnow. f) As e), but for the December 2019 – March 2020 period. g) As e), but for the day-3 forecast. h) As f), but for the day-3 forecast.

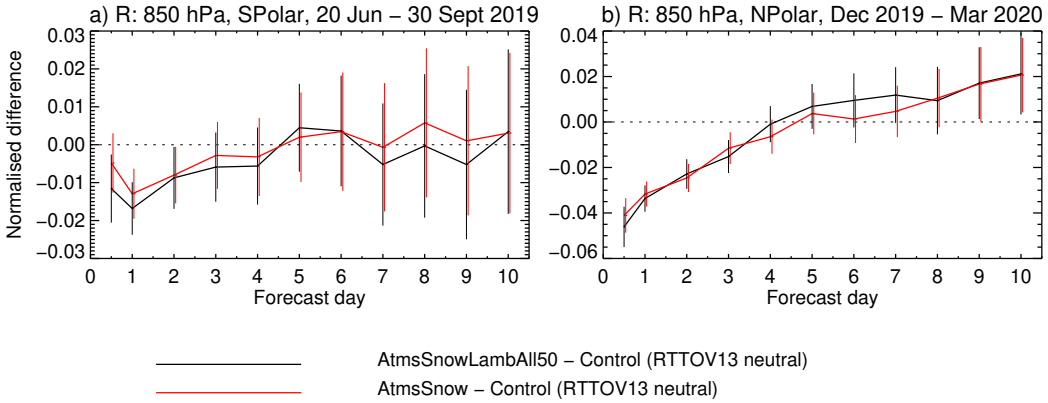

Figure 15: a) Normalised difference in the standard deviation of forecast error for relative humidity at 850 hPa as a function of forecast range for the AtmsSnow (read) and the AtmsSnowLamb (black) experiment relative to the Control over the South polar region (S of 60S) during the period 20 June - 30 September 2019. Each experiment has been verified against its own analysis. Vertical bars indicate 95 % confidence intervals. b) As a), but for the North polar region (N of 60N) for the December 2019 – March 2020 experiments.

able bias between observations and the background which is only partially reduced in the analyses. As the changes in humidity introduced through AtmsSnow and (to lesser extent) AtmsSnowLamb are in the same direction as the model bias, this, combined with regional variations, leads to apparently smaller forecast errors when each experiment is verified against its own analysis. The worsening of the bias as suggested by radiosondes is, however, still relatively small compared to the standard deviations of background or analysis departures, so it is not considered a major concern.

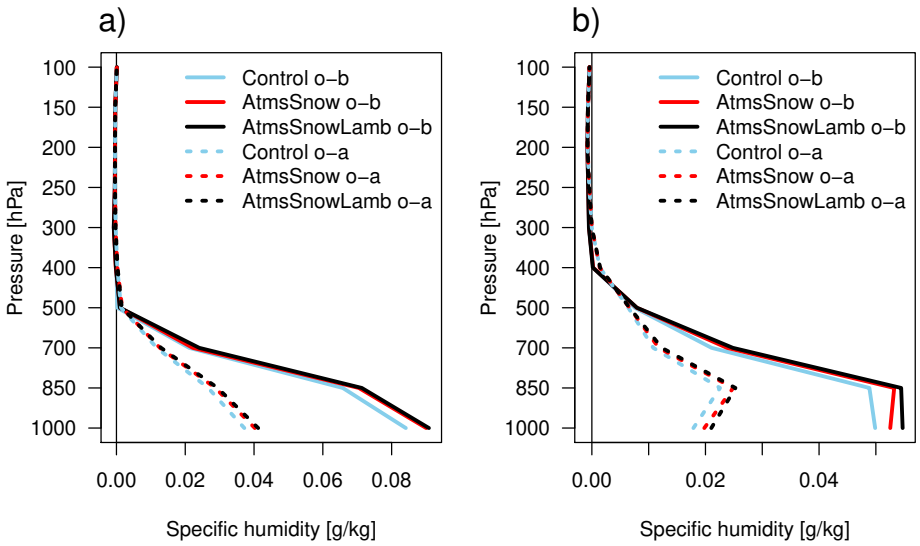

Figure 16: a) Bias in specific humidity for the background (solid) and the analyses (dashed) against radiosondes in the South polar region (S of 60S) for the period 20 June - 30 September 2019. Statistics are shown for the Control (blue), the AtmsSnow (red) and the AtmsSnowLamb (black) experiments. b) As a), but for the North polar region (N of 60N) for the December 2019 – March 2020 experiments.

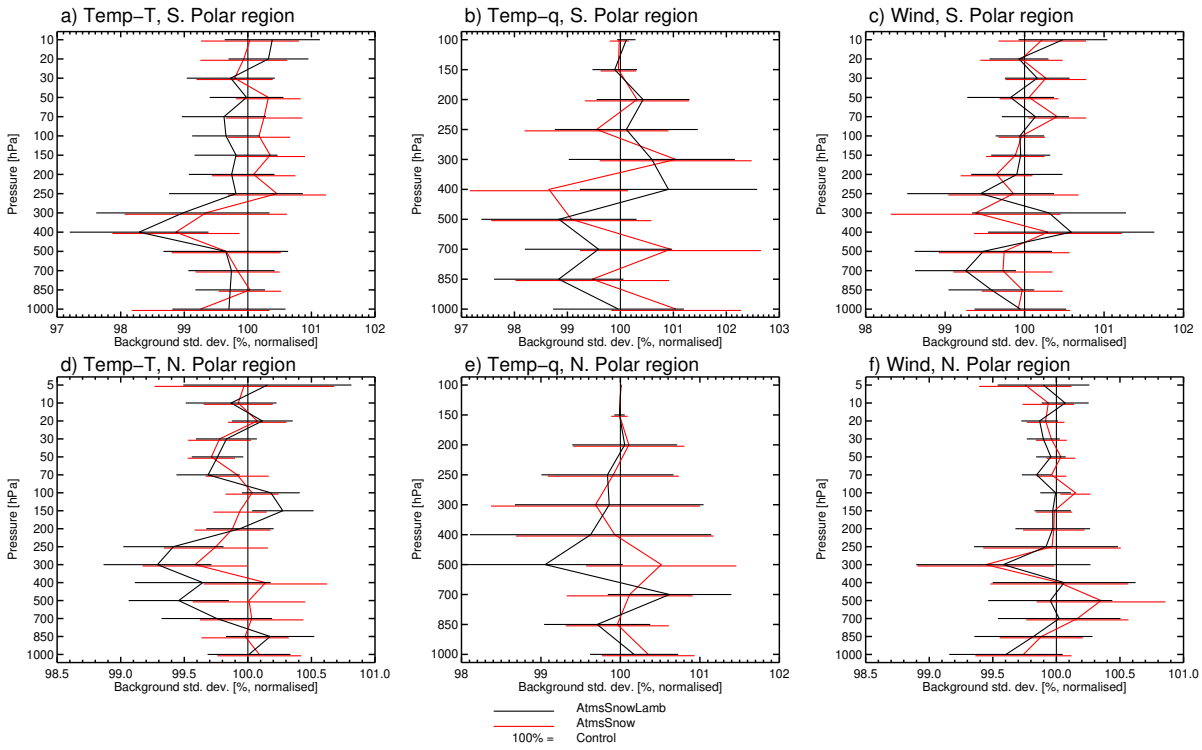

Figure 17: a) Standard deviations of background departures for temperature observations from sondes over the South polar region (south of 60S) for the 20 June – 30 September 2019 period. Values have been normalised by those of the Control experiment, and red lines indicate results from the AtmsSnow experiment, whereas black lines results for the AtmsSnowLamb experiment. Horizontal bars depict 95 % confidence intervals. b) As a), but for humidity observations. c) As a), but for wind observations. d) As a), but for the North polar region (north of 60N) and the December 2019 – March 2020 period. e) As d), but for humidity observations. f) As d), but for wind observations.

A neutral-to-slightly positive impact on short-range forecasts is also apparent from background departure statistics against conventional observations in the polar regions. Figure 17 shows a weak improvement in short-range forecasts in the lower and mid troposphere for the AtmsSnowLamb experiment over the Control, particularly for temperature over both polar regions in the respective winter months, but also for wind over the South polar winter. However, the signals are relatively weak, and only a few levels show statistically significant differences for the combined impact of adding the ATMS humidity-sounding channels and using a Lambertian assumption in the forward modelling. Results for the individual contributions are mostly not statistically significant by these measures.

5 Conclusions

This memorandum has investigated two aspects to increase and improve the use of microwave sounding data over snow and sea-ice, namely through the activation of humidity-sounding channels of ATMS over snow-covered land surfaces, as well as through more adequate forward modelling by taking Lambertian surface characteristics into account. The main findings are:

- Departure statistics obtained by treating snow and sea-ice surfaces as specular show viewing-angle

dependent biases that can be significantly reduced by using a Lambertian or semi-Lambertian assumption. This is particularly the case for the 183-GHz humidity-sounding channels for which fully Lambertian reflection characteristics appear to be a better approximation throughout the year. For the 50-GHz temperature-sounding channels, the degree of Lambertianity appears to be more variable seasonally and geographically, and there are also indications that biases introduced by using the top-level model surface temperature as effective skin-temperature play a significant role.

- The addition of the 183-GHz humidity channels of ATMS with a dynamic emissivity-retrieval approach gives a neutral to positive forecast impact at higher latitudes, regardless of whether a specular or Lambertian reflection is used.
- Treating snow and sea-ice surfaces as Lambertian reflectors for 183 GHz channels and semi-Lambertian for 50-GHz channels leads to neutral to positive forecast impact at higher latitudes. The improved forward modelling allows the assimilation of additional observations for the affected channels.
- The combination of adding the humidity-sounding channels of ATMS over snow and the introduction of the Lambertian treatment over snow and sea-ice gives overall a small positive impact at high latitudes, with some statistically significant benefits out to the day-3 forecast.

The present results are an example of achieving better impact from surface-sensitive satellite radiances from an extended use over snow and sea-ice surfaces and a better modelling of the surface-characteristics in the radiative transfer. The work follows the wider "all-surface" strategy pursued for MW radiances and other satellite data at ECMWF for many years. Most MW sounding radiances are now assimilated over all surfaces, with the exception of high orography, as well as snow and sea-ice surfaces for the most surface-sensitive channels. The findings show that improvements are still possible in the forward-modelling for these radiances, even with a relatively simple description of the surface characteristics for these surfaces.

The results have been obtained using the clear-sky assimilation route for MW sounders, but the results regarding the Lambertian reflection characteristics should also apply to the all-sky treatment of MW sounding radiances. The use of Lambertian characteristics in the all-sky assimilation will require developments in the radiative transfer model RTTOV-SCATT. While the parameterisation adopted in the present study offers a starting point, representing non-specular reflection in the context of a scattering atmosphere may need further refinements. Given that most MW sounding instruments with 183 GHz channels are assimilated through the all-sky route in the ECMWF system, and these channels showed particularly clear benefits from assuming Lambertian rather than specular reflection, improving on the specular assumption in RTTOV-SCATT is expected to be particularly beneficial,

Some of the short-comings and limitations of the approaches presently used to assimilate MW radiances over snow and sea-ice in the clear-sky or all-sky approach have also been exposed. Currently, the assimilation uses a relatively simple description of the surface-characteristics through an effective skin temperature, a retrieved emissivity, and fixed assumptions on reflection characteristics for these surfaces. There are indications that the model surface temperature is not a good first guess for the effective skin temperature, at least for the 50-GHz channels, as penetration effects are neglected. The use of a fixed assumption for the reflection characteristics is relatively crude, and a seasonally and geographically varying assumption may be more appropriate, especially for the 50-GHz channels. The interplay between reflection assumptions, biases in the skin-temperature, and biases in the retrieved surface emissivity leads to complex error characteristics which are not easy to untangle. Related to this, the current assimilation approach over snow and sea-ice relies on ad-hoc quality control procedures to avoid some

adverse effects from poor forward-modelling of the surface characteristics. While these were necessary in the past to obtain the desired impact, they will need to be revisited and adapted accordingly as the surface-representation improves. Further, in the present experiments, the skin-temperature sink variable acts to mitigate against errors in the surface-description. While this helps to avoid negative effects from the biases seen in the present experiments, it is likely reducing the amount of information that is extracted from the observations for the atmospheric analysis. Similarly, it probably also limits the benefits that can be obtained from a better description of the surface characteristics in the radiative transfer. It remains a challenge to improve these short-comings in the current pragmatic representation of the surface contributions and developed assimilation approaches.

There are several options to further improve the description of the surface contribution for atmospheric radiances and their assimilation, and the results from the present study provide some motivation that this should lead to further benefits. Possible approaches range from a better retrieval of surface information as part of the atmospheric analysis while staying with a simplified representation, to making use of information available from other Earth-System models as part of the coupled Earth System Assimilation developed at ECMWF. As an example for the former approach, the estimation of the effective skin temperature, surface emissivity and reflection properties could be improved in the atmospheric system, by estimating these quantities simultaneously during the assimilation, rather than sequentially or offline as in the present study. This would require exploiting better constraints offered through several instruments, viewing angles, and different frequencies and polarisations, for instance by adopting an augmented control variable approach like the one currently under investigation for skin-temperature (Massart et al. 2021). However, simultaneous estimation of skin-temperature, surface emissivity, and reflection properties is likely to be challenging due to similarities in the signal and difficulties in modelling the associated uncertainties. It would also require an adequate representation of key characteristics, for instance, in the case of emissivity the spectral, polarisation, and viewing angle dependencies. An alternative, possibly complementary approach is to make use of information available from other Earth System components in a coupled system, such as using information from the multi-layer snow model recently developed (Arduini et al. 2019) or information on the state of the sea-ice. Ideally, this would be based on physical modelling of the surface characteristics in a coupled radiative transfer model, including the representation of penetration effects and reflection characteristics. However, as a complete description of all relevant surface variables is likely to be elusive, the exploitation of statistical or machine learning methods may offer opportunities. Forward modelling of surface contributions from relevant Earth-System components would also open the door to using better the surface information contained in radiances that so far have only been exploited in the atmospheric system. This is particularly attractive for so-called "interface observations" with strong sensitivity to different components of the Earth System, such as MW window channels. The resulting better description of the surface contributions should also result in synergistic benefits in the use of MW sounding observations for the atmosphere.

A Lambertian approximation

A.1 Opacity-dependence of the effective zenith angle used in the Lambertian calculations

Mätzler (1987) proposed the use of an effective zenith angle in the calculation of the down-welling radiation to approximate Lambertian surface behaviour. The approximation is derived by integrating the down-welling contribution over a semi-sphere, assuming a homogeneous atmosphere. The effective zenith angle θ_{eff} is dependent on the atmospheric extinction at nadir (or zenith opacity) $\tau(z_0, z_1) =$

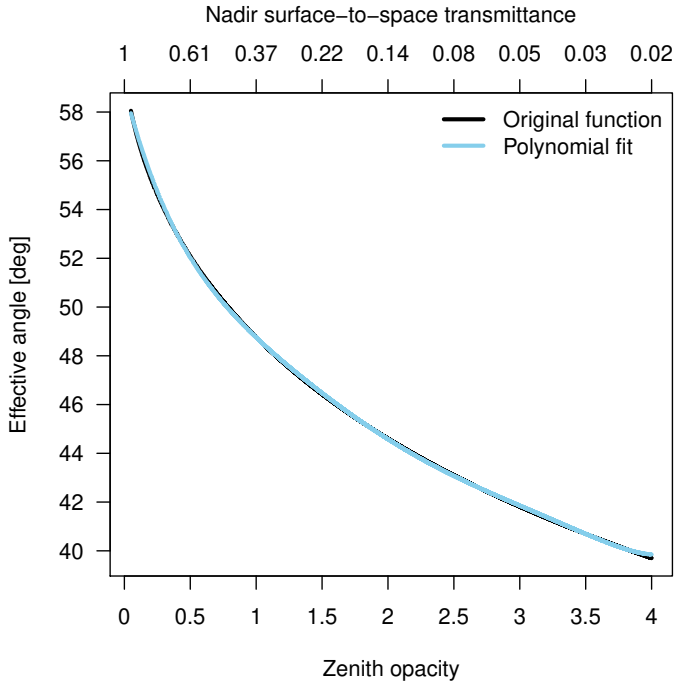

Figure 18: The original function (black) for the effective zenith angle $\theta_{eff}(\tau)$, together with the result of the polynomial fit (blue).

$\int_{z_0}^{z_1} \alpha(z)dz$ (where $\alpha(z)$ is the atmospheric absorption at altitude z), as given by:

$$\theta_{eff}(\tau) = \arccos\left(\frac{-\tau}{\ln(2\,\mathrm{E}_3(\tau))}\right) \tag{1}$$

where E_3 is the exponential integral of order 3.

For computational reasons, the effective angle formula is approximated in the present work using the following 6th-order polynomial:

$$\begin{aligned}\theta_{eff}(\tau) \approx 1.029024 - 0.367866\,\tau + 0.344010\,\tau^2 \\ -0.219791\,\tau^3 + 0.078976\,\tau^4 - 0.014515\,\tau^5 + 0.001061\,\tau^6\end{aligned} \tag{2}$$

The polynomial has been derived through a least-squares fit to the original function values over the interval 0.0001 to 4.2, sampled at 0.0001 intervals. The approximation makes an error of less than 0.003 rad (0.17°) for values of τ between 0.05 and 4. The original function and the polynomial fit are shown in Fig. 18.

A.2 Scan-dependent statistics with simplified representation of Lambertian behaviour

The results presented in this memorandum have been obtained with the polynomial fit to the effective zenith angle function as outlined in the previous appendix. The capability to do this is included in

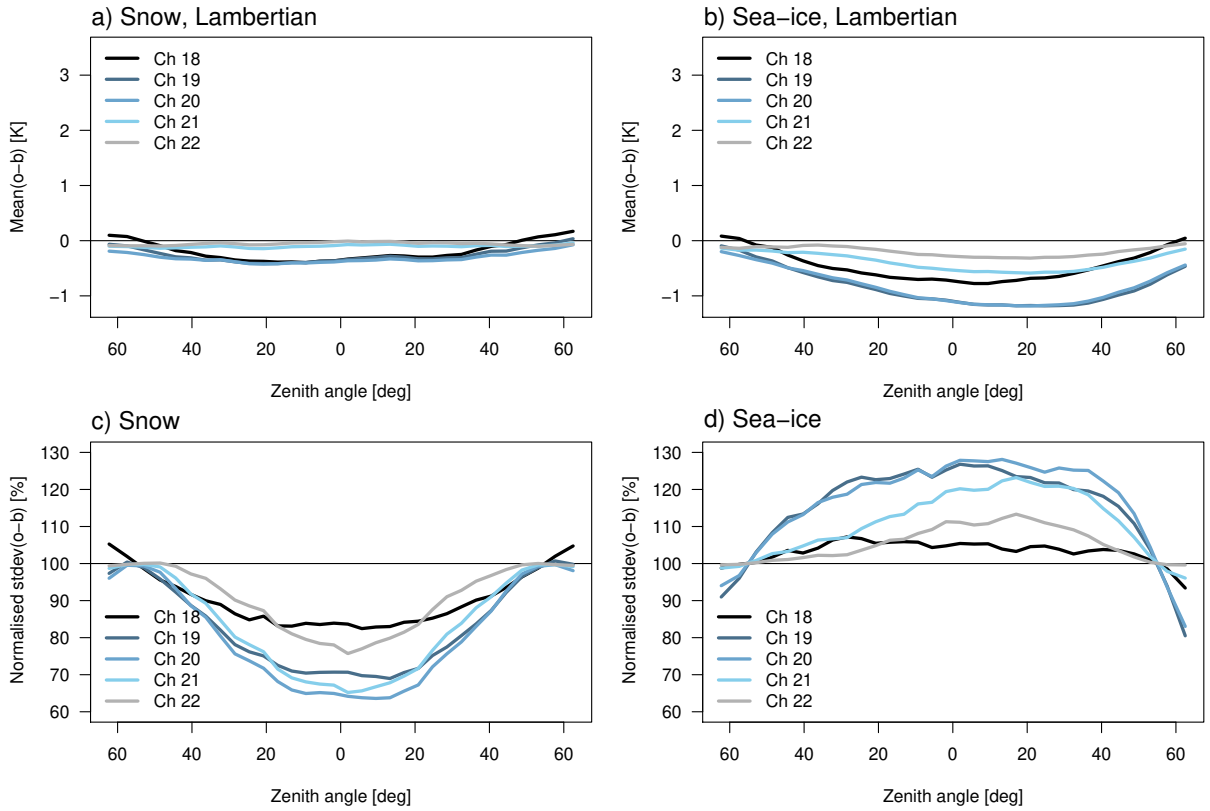

Figure 19: a) Mean departures (after bias correction) over snow-covered surfaces over land as a function of scan-position for S-NPP ATMS channels 18 to 22 for January 2017 when the Lambertian assumption is used, approximated using a fixed 55°effective zenith angle for the computations of the down-welling radiations. The Figure is labelled on the x-axis with the average zenith angle per scan-position. b) As a), but for sea-ice surfaces. c) Standard deviation of background departures obtained using the Lambertian approximation with the fixed effective zenith angle, normalised by values obtained using the specular assumption [%]. Data are displayed as a function of scan-position for ATMS channels 18 to 22 for snow-covered surfaces and January 2017. d) As c), but for sea-ice surfaces. The Figure can be compared to similar statistics shown in Fig. 1c-f, for which the zenith-opacity of the effective angle has been taken into account (note the different y-axes for the lower panels).

RTTOV version 13. For comparison, we provide here as well results for a simplified approximation of the Lambertian effect, in which the effective zenith angle is set to a fixed value of 55°. This is the approximation made by Guedj et al. (2010) and available in RTTOV from version 11 onwards. As can be seen from Fig. 18, this choice of effective zenith angle is most appropriate for strongly surface-sensitive channels, with a surface-to-space transmittance > 0.6. This is appropriate, for instance, for channel 3 of ATMS, which is used in the surface emissivity retrieval for 50 GHz channels over land or sea-ice. However, the sounding channels presently assimilated at ECMWF have weaker surface-sensitivity, and smaller effective zenith angles are more appropriate for these. The weaker the surface-dependence, the less important the characteristics of the surface reflection become, so by choosing a fixed angle appropriate for channel 3 it was assumed that the choice of effective angle matters less for the less surface-sensitive channels.

For comparison with the results presented in section 3, we present here scan-dependent statistics for the case of using a fixed 55°effective zenith angle in the Lambertian calculations for 50 and 183 GHz channels. Comparing Figures 1 and 19 suggests that taking the dependence of the effective zenith angle on

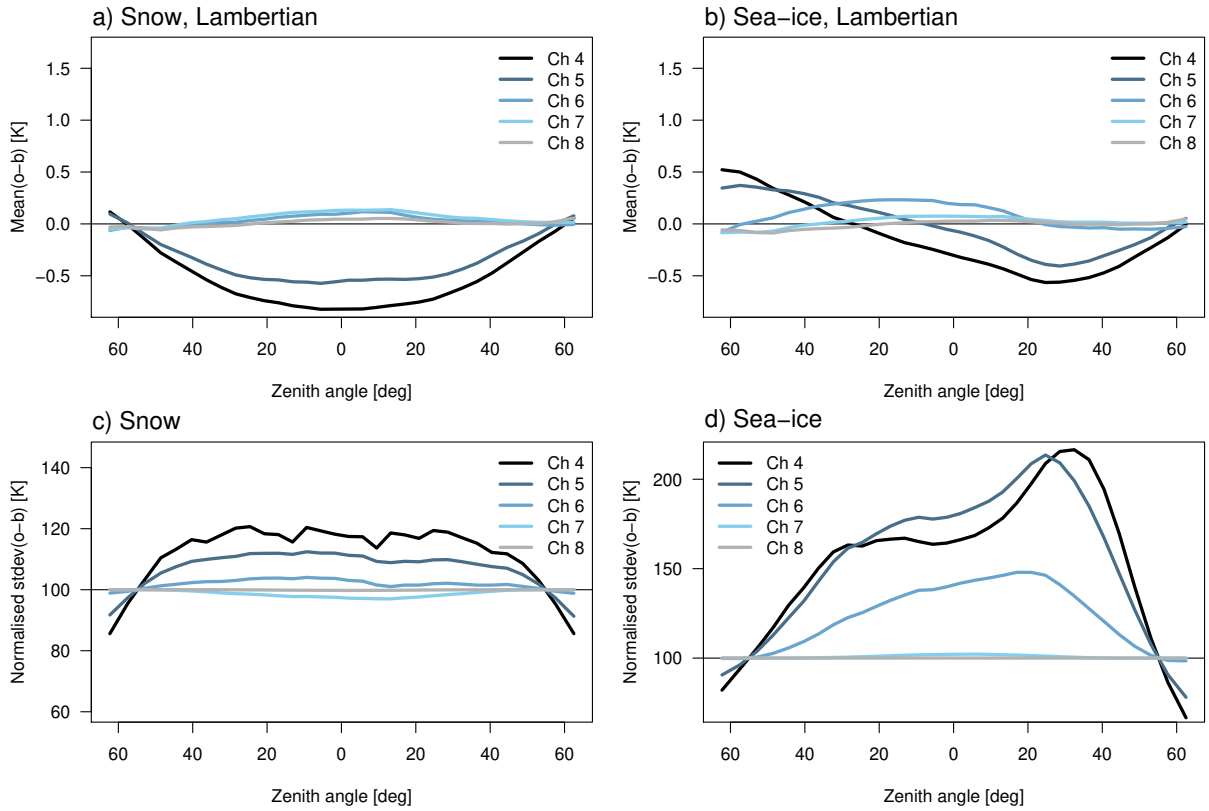

Figure 20: As Fig. 19, but for the S-NPP ATMS channel 4 to 8. The Figure can be compared to similar statistics shown in Fig. 4c-f, for which the zenith-opacity of the effective angle has been taken into account (note the different y-axes for the lower panels).

the zenith opacity into account has overall a relatively small effect on the bias statistics for the 183 GHz channels. Some benefits can be seen in the standard deviation statistics over sea-ice, for which the fixed effective zenith angle shows larger values. The situation is different for the 50 GHz channels (cf Figures 4 and 20), for which there appears to be a sizeable effect, particularly for the lowest-peaking channels considered (channels 4 and 5), both in terms of the bias as well as the standard deviation of departures. The statistics suggest that taking the dependence on the zenith opacity into account leads to better results for these channels for the period and hemisphere in question when a fully specular assumption is used. However, as shown in Fig. 5 there also appear to be seasonal variations in the degree of Lambertian behaviour for the 50 GHz channels, and this aspect is not considered here.

Acknowledgements

Thanks go to James Hocking (Met Office) for including the updated Lambertian capability in RTTOV-13. The ECMWF system used in this study is the result of developments of a large number of staff over many years, and their contributions to this work are gratefully acknowledged.

References

Arduini, G., G. Balsamo, E. Dutra, J. Day, I. Sandu, S. Boussetta, and T. Haiden, 2019: Impact of a multi-layer snow scheme on near-surface weather forecasts. *Journal of Advances in Modeling Earth Systems*, **11**, 12, 4687–4710.

Bormann, N., 2017: Slant path radiative transfer for the assimilation of sounder radiances. *Tellus A: Dynamic Meteorology and Oceanography*, **69**, 1, 1272779.

Bormann, N., A. Fouilloux, and W. Bell, 2013: Evaluation and assimilation of ATMS data in the ECMWF system. *J. Geophys. Res.*, **118**, 12,970–12,980, doi: 10.1002/2013JD020325.

Bormann, N., H. Lawrence, and J. Farnan, 2019: Global observing system experiments in the ECMWF assimilation system. Technical Memorandum 839, ECMWF, Reading, UK.

Bormann, N., C. Lupu, A. Geer, H. Lawrence, P. Weston, and S. English, 2017: Assessment of the forecast impact of suface-sensitive microwave radiances over land and sea-ice. *ECMWF Technical Memorandum*, 804.

Di Tomaso, E., and N. Bormann, 2012: Assimilation of ATOVS radiances at ECMWF: second year EUMETSAT fellowship report. EUMETSAT/ECMWF Fellowship Programme Research Report 26, ECMWF, Reading, U.K., 27 pp.

Duncan, D., and N. Bormann, 2020: On the addition of microwave sounders and NWP skill, including assessment of FY-3D sounders. EUMETSAT/ECMWF Fellowship Programme Research Report 55, ECMWF, Reading, U.K.

Geer, A., F. Baordo, N. Bormann, S. English, M. Kazumori, H. Lawrence, P. Lean, K. Lonitz, and C. Lupu, 2017: The growing impact of satellite observations sensitive to humidity, cloud and precipitation. *Q. J. R. Meteorol. Soc.*, **143**, 3189–3206. doi:10.1002/qj.3172.

Guedj, S., F. Karbou, F. Rabier, and A. Bouchard, 2010: Toward a better modeling of surface emissivity to improve AMSU data assimilation over Antarctica. *IEEE Trans. Geosci. Remote Sensing*, **4**, 1976–1985.

Harlow, R., 2009: Millimeter microwave emissivities and effective temperatures of snow-covered surfaces: Evidence for Lambertian surface scattering. *IEEE Transactions on Geoscience and Remote Sensing*, **47**, 7, 1957–1970.

Karbou, F., E. Gérard, and F. Rabier, 2006: Microwave land emissivity and skin temperature for AMSU-A and -B assimilation over land. *Q. J. R. Meteorol. Soc.*, **132**, 2333–2355.

Lawrence, H., and N. Bormann, 2014: First year report: The impact of HIRS on ECMWF forecasts, adding ATMS data over land and sea ice and new observation errors for AMSU-A. EUMETSAT/ECMWF Fellowship Programme Research Report 34, ECMWF, Reading, U.K., 36 pp.

Lawrence, H., N. Bormann, and S. English, 2014: Scene-dependent observation errors for the assimilation of AMSU-A. EUMETSAT/ECMWF Fellowship Programme Research Report 39, ECMWF, Reading, U.K., 30 pp.

Lawrence, H., N. Bormann, I. Sandu, J. Day, J. Farnan, and P. Bauer, 2019: Use and impact of Arctic observations in the ECMWF Numerical Weather Prediction system. *Q. J. R. Meteorol. Soc.*, **145**, 725, 3432–3454.

Lawrence, H., J. Goddard, I. Sandu, N. Bormann, P. Bauer, and L. Magnusson, 2019b: An assessment of the use of observations in the Arctic at ECMWF. Technical Memorandum 845, ECMWF, Reading, UK.

Liu, Q., F. Weng, and S. English, 2011: An improved fast microwave water emissivity model. *IEEE Trans. Geosci. Remote Sens.*, **49**, 1238–1250.

Massart, S., N. Bormann, M. Bonavita, and C. Lupu, 2021: Multi-sensor analyses of the skin temperature for the assimilation of satellite radiances in the european centre for medium-range weather forecasts (ecmwf) integrated forecasting system (ifs, cycle 47r1). *Geoscientific Model Development Discussions*, **2021**, 1–30.

Mätzler, C., 1987: Applications of the interaction of microwaves with the natural snow cover. *Remote Sens. Rev.*, **2**, 259–387.

Mätzler, C., and P. Rosenkranz, 2007: Dependence of microwave brightness temperature on bistatic surface scattering: Model functions and application to AMSU-A. *IEEE Trans. Geosci. Remote Sensing*, **45**, 2130–2138.

Rosenkranz, P., and C. Mätzler, 2008: Dependence of AMSU-A brightness temperatures on scattering from Antarctic firn and correlation with polarization of SSM/I data. *IEEE Geosci. Remote Sensing Letters*, **5**, 769–773.

Weston, P., and N. Bormann, 2018: Enhancements to the assimilation of ATMS at ECMWF: Observation error update and addition of NOAA-20. EUMETSAT/ECMWF Fellowship Programme Research Report 48, ECMWF, Reading, U.K., 28 pp.

Weston, P., N. Bormann, A. Geer, and H. Lawrence, 2017: Harmonisation of the usage of microwave sounder data over land, coasts, sea-ice and snow: First year report. EUMETSAT/ECMWF Fellowship Programme Research Report 45, ECMWF, Reading, U.K.